AD NUMBER

AD489344

NEW LIMITATION CHANGE

TO

Approved for public release, distribution unlimited

FROM

Distribution authorized to U.S. Gov't. agencies and their contractors; Administrative/Operational Use; JAN 1966. Other requests shall be referred to Air Force Aero Propulsion Lab., AFSC, Wright-Patterson AFB, OH 45433.

AUTHORITY

AFAPL ltr, 12 Apr 1972

AFAPL-TR-66-2
Part I

UTILIZATION OF ELASTIC RECOVERY MATERIALS FOR THE DEVELOPMENT OF CREW TRANSFER TUNNELS, AIRLOCKS, AND SPACE MAINTENANCE HANGARS

Part I. Space Maintenance Hangar Design Study

T. L. Hoffman
Goodyear Aerospace Corporation

TECHNICAL REPORT AFAPL-TR-66-2, PART I

January 1966

Air Force Aero Propulsion Laboratory
Research and Technology Division
Air Force Systems Command
Wright-Patterson Air Force Base, Ohio

NOTICES

When Government drawings, specifications, or other data are used for any purpose other than in connection with a definitely related Government procurement operation, the United States Government thereby incurs no responsibility nor any obligation whatsoever; and the fact that the Government may have formulated, furnished, or in any way supplied the said drawings, specifications, or other data, is not to be regarded by implication or otherwise as in any manner licensing the holder or any other person or corporation, or conveying any rights or permission to manufacture, use, or sell any patented invention that may in any way be related thereto.

Qualified users may obtain copies of this report from the Defense Documentation Center (DDC), Cameron Station, Bldg. 5, 5010 Duke Street, Alexandria, Virginia, 22314.

The distribution of this report is limited because it contains comparative data on commercial products tested for applications other than intended by the manufacturer.

Copies of this report should not be returned to the Research and Technology Division unless return is required by security considerations, contractual obligations, or notice on a specific document.

UTILIZATION OF ELASTIC RECOVERY MATERIALS FOR THE DEVELOPMENT OF CREW TRANSFER TUNNELS, AIRLOCKS, AND SPACE MAINTENANCE HANGARS

Part I. Space Maintenance Hangar Design Study

T. L. Hoffman

FOREWORD

This report was prepared by Goodyear Aerospace Corporation, Akron, Ohio under United States Air Force Contract Number AF33(615)-2114. The Goodyear Aerospace Corporation report identification is GER-12348. The work was administered under the direction of the Aero Propulsion Laboratory. Mr. F.W. Forbes and Lt. A.J. Zappanti of this laboratory (APFT) were project engineers for the Air Force.

The program began in May 1965 and was concluded in October 1965 with submittal of the final report in December 1965. The program was directed by the Space Systems and Analytics Division, managed by Mr. S.J. Pipitone, of Goodyear Aerospace Corporation.

This program was a group effort headed by Mr. L. Jurich, project manager, of the Astronautics Programs Department with the special assistance of T.L. Hoffman, project engineer; K.L. Cordier, materials; B.H. Burzlaff, environmental effects; R.L. Ginter, thermodynamics; and J.E. Houmard, structural analysis.

This report was submitted by the author January 1966.

This report contains no classified information extracted from other classified documents.

This technical report has been reviewed and is approved.

James A. McMillan, Major, USAF
Chief, Space Technology Branch
Support Technology Division

ABSTRACT

This report summarizes the preliminary design and analysis performed by Goodyear Aerospace Corporation on the Space Maintenance Hangar expandable structures experiment for MOL under Air Force Contract Number AF33(615)-2114 for the Air Force Aero Propulsion Laboratory. The program established the preliminary design, supported by preliminary analysis, of a 9-foot diameter cylindrical structure with an expanded length of 25 feet which attaches to the aft end of the MOL to serve as a pressurized meteoroid protective enclosure for astronauts working on MOL experiments. The expandable hangar construction is a composite wall consisting of an inner triple-barrier pressure bladder for gas retention, a web strap structural layer, a 2-inch thick polyether foam meteoroid barrier, and a film-cloth laminate outer cover with a thermal coating.

The web straps carry the longitudinal presure loads while the circumferential pressure loads are distributed from the web straps to a series of intermittently-spaced wire cable circumferential hoops. Flexible clam shell doors mounted to rigid frames at the aft end of the hangar can be opened and closed by a reel and cable system to provide an opening for large objects to pass thru when the hangar is unpressurized. The extended length of the hangar is maintained when unpressurized by 3 inflated 10 inch diameter full length deployment tubes while the shape is maintained by the foam barrier. Fabrication of the hangar, which is estimated to weigh 1459 pounds including the packaging canister, is entirely feasible and within the present state of the art.

TABLE OF CONTENTS

TABLE OF CONTENTS (Continued)

LIST OF ILLUSTRATIONS

LIST OF TABLES

LIST OF SYMBOLS

THERMAL ANALYSIS - SECTION VII

a	Albedo constant for earth
C	Solar constant (Btu/hr-ft^2)
C_p	Specific heat (Btu/lb-$^\circ$F)
E	Earth radiation intensity (Btu/hr-ft^2)
F_c	Radiation view factor from cylindrical surface to earth
F_e	Radiation view factor from end surface to earth
F_h	Radiation view factor from hemispherical surface to earth
F_β	Radiation view factor from surface at orientation angle β to earth
f_1, f_2	Functions defined in text
h_o	Orbital altitude (miles)
K	Dimensionless altitude parameter
K_t	Thermal conductivity (Btu-in./hr-ft^2-$^\circ$F)
Q	Albedo radiation intensity (Btu/hr-ft^2)
R_e	Earth radius (miles)
S	Solar radiation intensity (Btu/hr-ft^2)
T	Temperature ($^\circ$R)
T_i	Temperature of node i ($^\circ$R)
w	Mass (lb/ft^2)
$(wc_p)_i$	Thermal mass of node i (Btu/ft^2-$^\circ$F)
Y	Distance between foam nodes (inches)
α	Solar absorptance
β	Orientation angle of surface with respect to earth (radians)
ϵ	Emittance (infrared absorptance)
ϵ_I	Effective emittance between bumper wall and outer laminate
ϵ_1, ϵ_2	Emittances of interface surfaces
θ	Angle about earth from earth-sun line (radians)
ρ	Density (lb/ft^3)
τ	Time (hours)

SUBSCRIPTS

c	Cylindrical surface
e	End surface
g	Garage
h	Hemispherical surface
θ	At orientation angle
n	Node number

STRUCTURAL ANALYSIS - SECTION VIII

C	Constant, defined in text
d	Wire diameter (in.)
E	Modulus of elasticity (psi)
F, F_2	Longitudinal components of the strap tension at its ends (lbs)
F.S.	Factor of safety
F_{tu}	Ultimate tensile strength (lbs or psi)
f_m, f_c	Calculated meridional and circumferential stress respectively (lb/in. or psi)
K	Constant, defined in text
ℓ	Length of the chord of the circular arc of the deformed longitudinal strap (in.)
N	Number of longitudinal strap or number of meridional cables in the end closure
n	Number of strands in hoop cables
P	Radial load on hoop cable (lb)
P_u	Ultimate load applied to the part of interest (lb)
p	Pressure (psi)
R	Mean radius of the hoop cable (in.)
r	Radius of the circular arc of the deformed longitudinal strap and the deformed bladder (in.)
r_o, r_i	Outer and inner radii of the cylindrical part of the shelter, respectively

LIST OF SYMBOLS (Continued)

T	Tension load in a longitudinal strap of the inflated cylinder or in a cable (lb)
T_m	Tension load in the meridional cables (lb)
w	Distributed pressure loading on a longitudinal strap (lb/in.)
x, y	Cartesian coordinates defined by sketches of figures (in.)
x, y, z, k_1, k_2, β, γ	Quantities used in determining the location of the outer hoop cables (defined by sketch)
x_i	Nominal diameter of the apex ring (spider) (in.)
x_o	Effective outer diameter of the clamping rings (in.)
x_o, y_o	Coordinates of the end closure at its juncture with the conical frustrum (in.)
x_t, y_t	Semi-major and semi-minor axes of the isotensoid end closure, respectively (in.)
α	Angle that the longitudinal straps of the cylinder make with hoop cables (degs)
ϵ	Strain (in./in.)
ϵ_u	Breaking strain (in./in.)
ζ	Angle between the initially straight strap and the chord of its circular arc after deformation (deg)
θ	Half of the central angle of the circular arc of the nonextensible deformed longitudinal strap (deg)
ρ_m, ρ_c	Principal meridional and circumferential radii of curvature, respectively (in.)
σ	Slope of the meridian of the end closure or Angle between the initially straight strap and the axis of the cylinder (deg)
σ_o	Slope of the meridian at the point x_o, y_o (deg)
λ	Variable quantity

SUBSCRIPTS

c	Isotensoid, meridian cables
l	Left-hand strap section
r	Right-hand strap section
u	Ultimate
5, 10	Denote the 5 and 10 psi pressure loadings, respectively

LIST OF SYMBOLS (Continued)

γ	Extensible strap angle
θ	Nonextensible strap angle
ϵ	Extensible shape constant

SECTION I

INTRODUCTION

A. GENERAL

The exposure of spacecraft to space environment for extended periods of time imposes numerous problems which must be resolved. Three areas of major concern, with reference to the extended time periods in space, are as follows:

(1) The dangers to personnel or subsystems from meteoroids.

(2) The temperature extremes.

(3) The high vacuum encountered.

The study report presents the results of Goodyear Aerospace Corporation's (GAC) program efforts conducted under Contract AF33(615)-2114 for the Air Force Aero Propulsion Laboratory (AFAPL). The contract effort was fundamentally directed toward the design of a space maintenance hangar for an expandable structures experiment for a Manned Orbital Laboratory (MOL). The secondary effort in the design was the alleviation of thermal shock and vacuum environment for personnel involved in activities in the hangar.

The program, which established a design and analysis of a pressurized enclosure for ultimate demonstration of the concept feasibility, was performed in two phases:

(1) Establishing concept definitions.

(2) Proceeding with the design and analyses.

A test program, paralleling the second phase, was conducted substantiating the structural material, the methods of fabrication, and the composite wall design for meteoroid protection.

The basic objectives of the program were the selection of materials, development of fabrication techniques and establishment of operational procedures. Material selection was directed toward materials which would offer specific resistance to meteoroid penetration and yet fabricate into a simple, erectable enclosure. Methods of fabrication for the materials also involved procedures for packaging, deploying, and pressurizing the enclosure. The mode of operation was based on the possible applications of the hangar.

The final effort of the program was the evolvement of development plans for the preprototype fabrication and testing, and for the flight hardware fabrication and testing.

B. CONCEPT CONSTRAINTS

In the design of the space maintenance hangar, certain constraints and requirements were stipulated by AFAPL. The structure was to be a flexible enclosure with a 7-foot minimum inside diameter and a 24-foot minimum length. The working pressure was to be a 5 psi differential with a test pressure differential of 10 psi. The total leak rate was not to exceed one-half pound of oxygen per day when the hangar was subjected to the working pressure. Packaging was to simulate stowage on the MOL without restriction of the launching operation. The hangar was to be self deploying with automatic pressurization and door operation.

Provisions had to be made on the hangar for meteoroid protection to the extent that the probability of zero penetration for a period of 60 days would exceed 0.995.

The enclosure exterior surface was to be coated to provide optimum temperatures inside the enclosure for humidity control, prevention of spacecraft systems degradation, and for habitation. The coating would also serve as a protection for the enclosure components. When

making the coating selection, it was to be assumed that the vehicle would be in a circular earth orbit of 160 nmi and rotating at a rate of 6 degrees per second.

The design would include a proposed method for pressure testing the enclosure, with attachments to a static test structure simulating the interface to the MOL.

To establish a space maintenance hangar with a more definite approach and one directed toward MOL System experiments without jeopardizing the program objectives, Goodyear Aerospace stipulated further requirements in concept definition:

(1) The enclosure would be adapted to existing hardware components, where possible, and employ a minimum amount of rework.

(2) Design of the concept would permit variable length enclosures without affecting structural characteristics.

(3) The concept structure would be limited to proven fabricating technology.

The program is also constrained by the space environmental conditons present in a 160 nautical mile earth orbit.

In the design, the following conditions were assumed: A solar flux of 443 Btu/sq ft/hr, and a maximum earth albedo heat flux of 160 Btu / sq ft/hr was used in the thermal analysis. For the micrometeoroid protection system, the flux versus mass spectrum information was in accordance with the MSC Engineering Criteria Bulletin EC-1 dated 8 November 1963. Because of the low energy levels, 6×10^6 rad for a 60-day period, radiation effects were not considered.

SECTION II

SUMMARY

A. GENERAL

The basic space maintenance hangar was designed as an integrated system for operation on a large manned orbiting space vehicle. It is comprised of a flexible structure, a rigid structure, clam shell doors, and components to accomplish deployment of the system. The hangar was configured to comply with the concept constraints listed in Section I and to be compatible with the MOL for orbiting the earth. The enclosure is packaged within the perimeter of the MOL transport (launch) vehicle. Except for air supply, power requirements, humidity control and peak thermal conditions, the system is fundamentally independent of the manned spacecraft. Because of the bay-type construction, the hangar is readily adapted to a decrease or increase in length.

B. SYSTEM DESCRIPTION

Basically, the space maintenance hangar is an accordion-shaped cylinder with a domed end. The enclosure has an overall length of 25 feet and a diameter of 9.1 feet. The hangar is attached to the head of the MOL space structure near the periphery of the cylinder. As shown in Figure 1, the accordion section is fabricated from flexible material and patterned to fold within the perimeter of an existing launch vehicle.

The aft portion of the flexible section mates with a rigid cone segment. This structure supports the door frames, the end closure, and the sealing system, and maintains a dimensional relationship between these related components. The segmented cone is integral with an adapter section structure. The cone serves the dual function of being a part of the space hangar in addition to being part of the packaging canister. Doors for the enclosure consist of two contoured frames positioned and hinged at the equator of the cone. Radiating from a spider fitting at the center of each door frame is a network of cables terminating at the cone periphery.

The enclosure system is operated with pneumatic and electrical power. Deployment of the structure is achieved through pressurization of the inflatable deployment tubes. Door closure is achieved by a cable system. Electrically powered reels, with cables, open the doors. The system is designed to function automatically in sequence from the initial deployment to pressurization of the enclosure.

C. METEOROID AND THERMAL CAPABILITY

Based on hypervelocity particle impact tests, a flexible polyether foam is used as a micrometeoroid barrier. To comply with the 60-day, 0.995 probability requirement the foam blanket is 2 inches thick with an 0.015-inch cloth outer cover.

For temperature control within the hangar, thermal coatings are applied to the cloth cover and cone segment. Under normal conditions the desired temperatures are maintained by the insulating properties of the meteor barrier in conjunction with the thermal control coating.

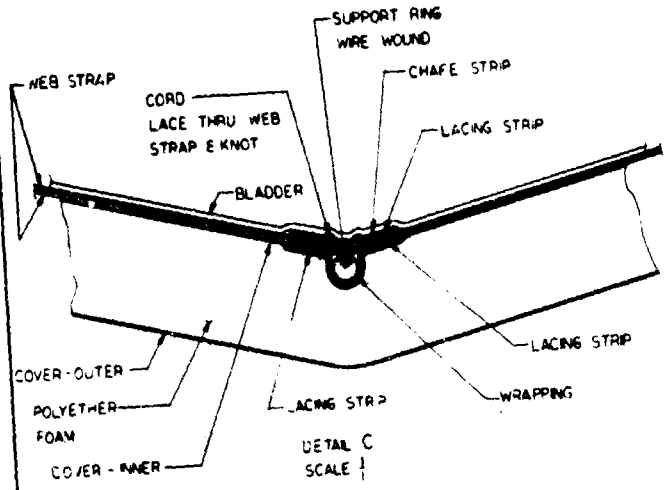

DETAIL C
SCALE 1/1

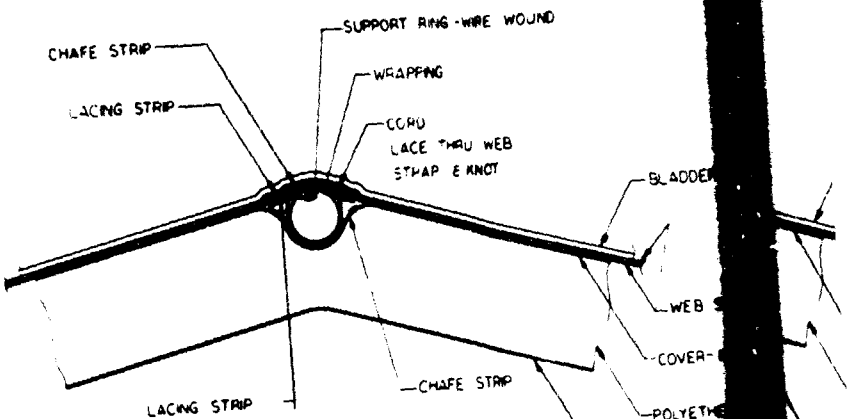

DETAIL B
SCALE 1/1

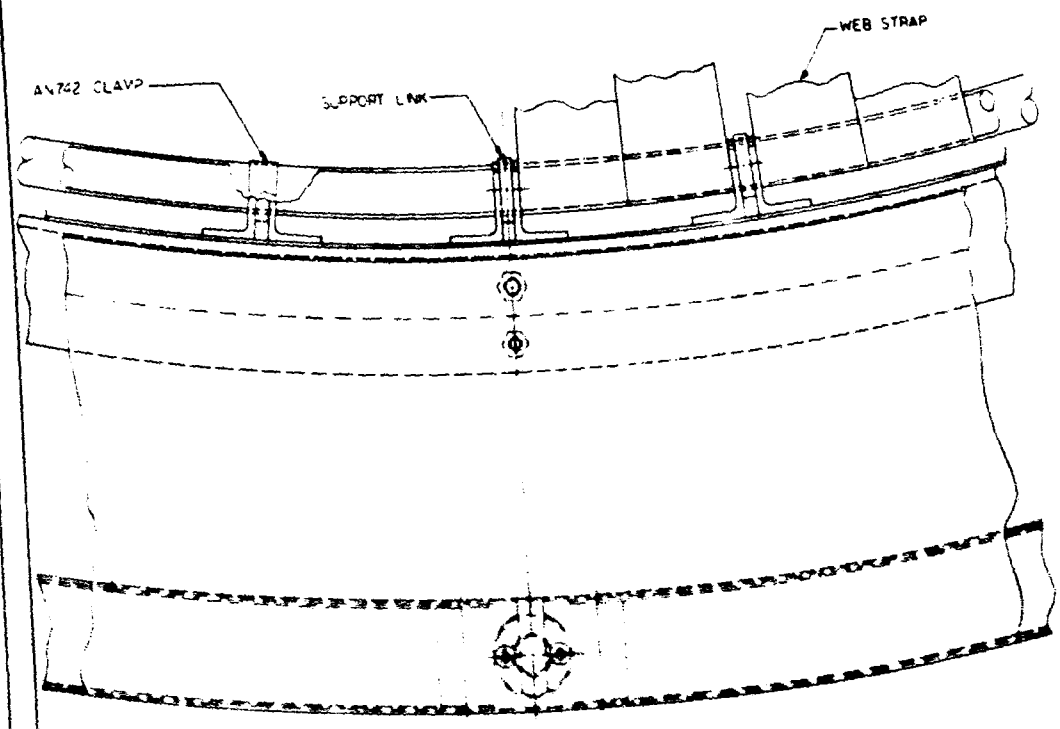

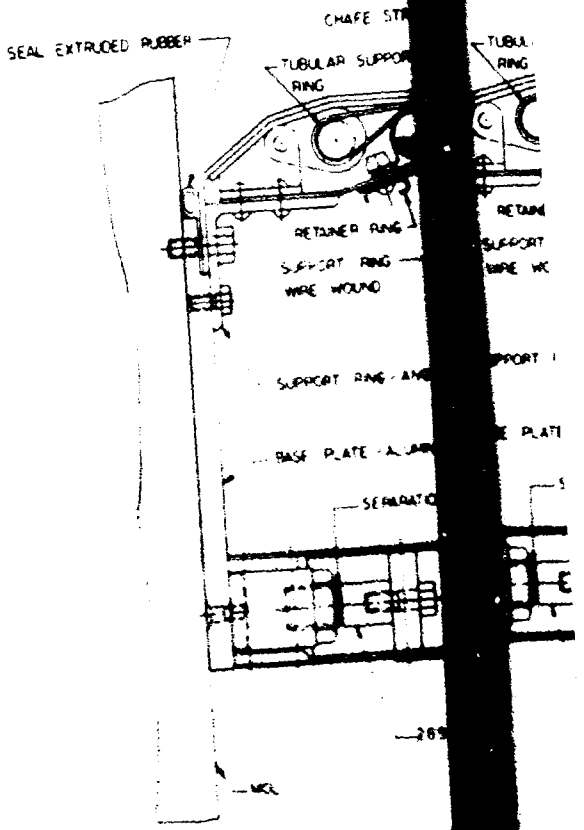

SECT
SCA

A

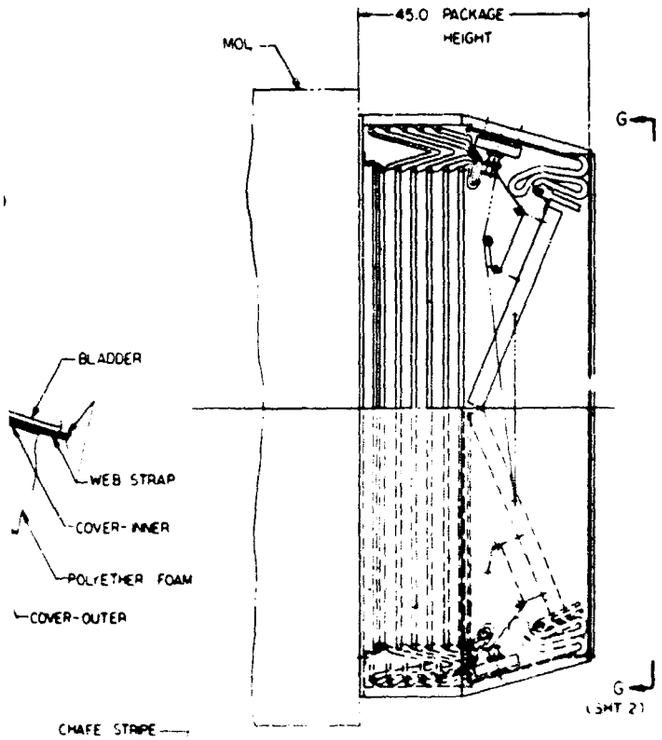

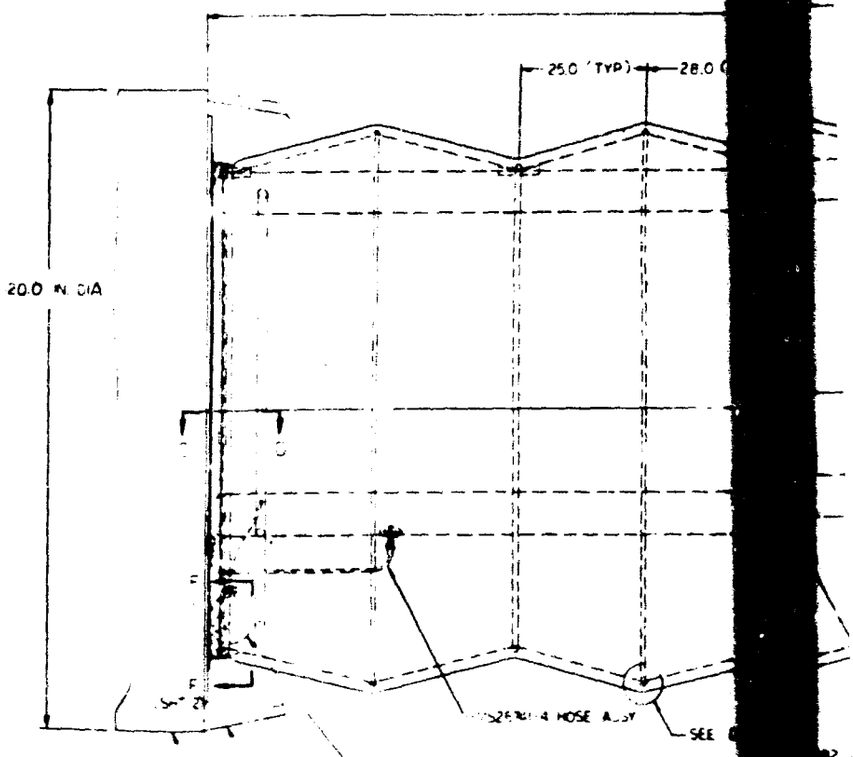

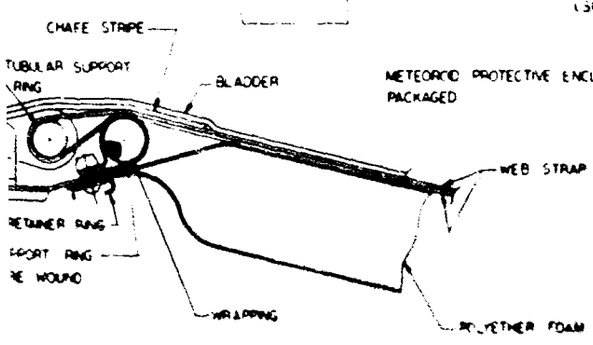

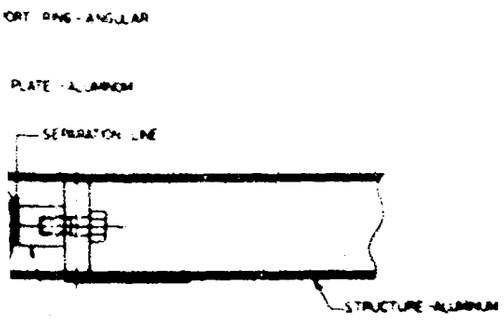

289 FRANGIBLE STUD
PROPELLEX CHROMALLOY CORP

SECTION D-D
SCALE

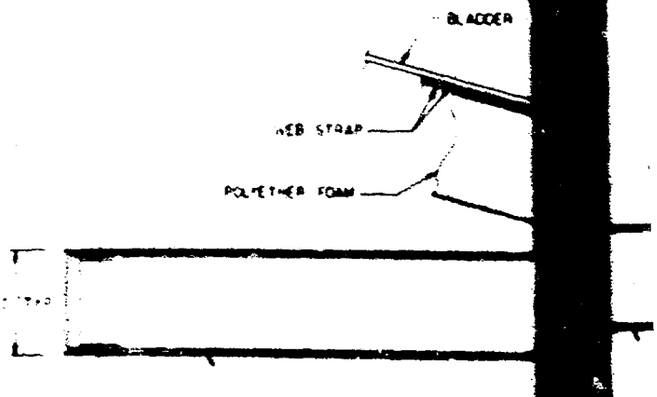

E9582 PRESSURE VESSEL-WALTER KIDDE 3000
84045 FITTING-WALTER KIDDE
AN832-4 UNION-BULKHEAD
1802-087-05 VALVE (NC) EXPLOSIVE CONAX CO
AF77C-512C VALVE SOLENOID ECKEL VALVE CO
AN832-4 UNION-BULKHEAD
29984-AM REGULATOR VALVE ASSY-MARROTT
VALVE CO

B

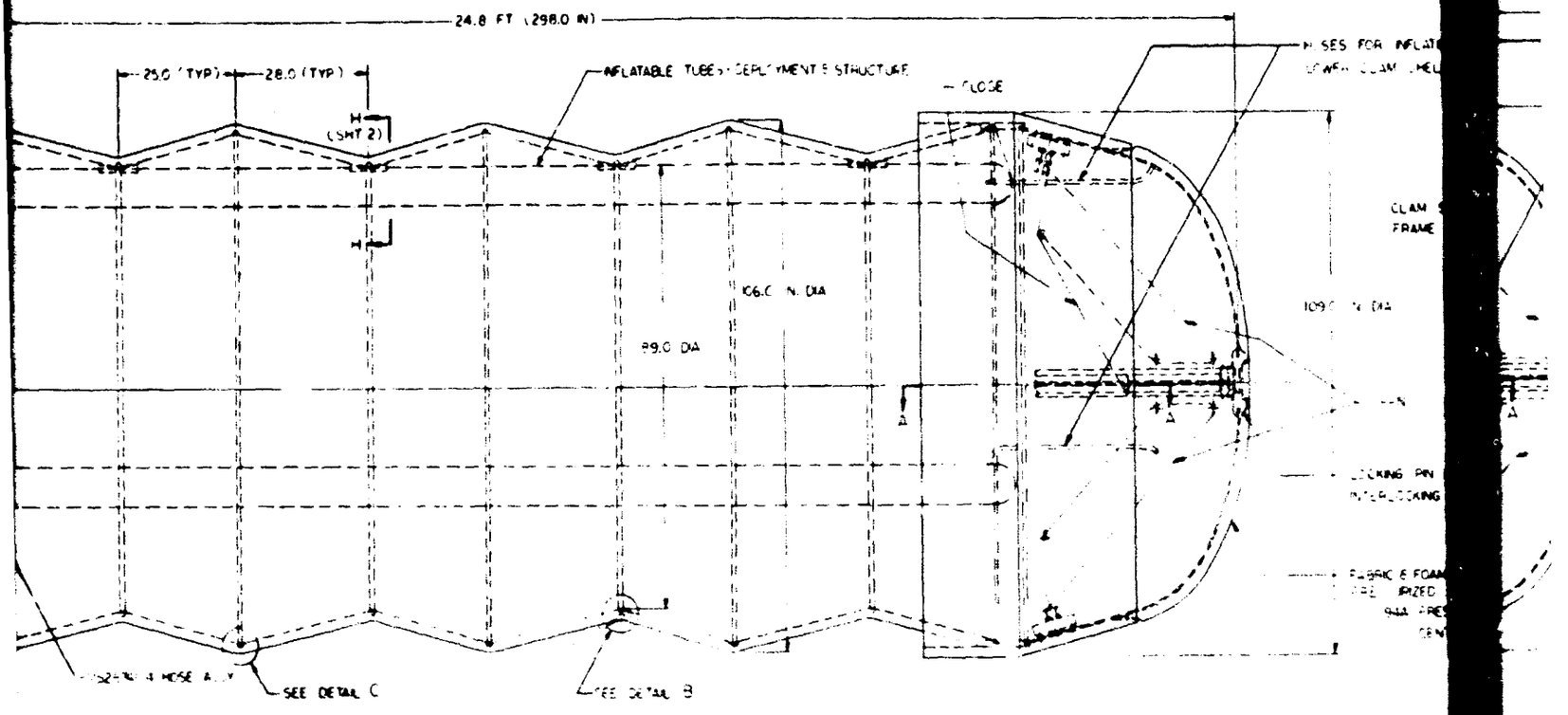

B2 PRESSURE VESSEL-WATER 4000 PSI 300 CU IN
4-5 FITTING-WATER 4000
132-4 UNION-BULKHEAD
8-087-05 VALVE NC EXPLOSIVE CONAX CORP
PPC-3460 VALVE SOLENOID ECKEL VALVE CO
B32-4 UNION-BULKHEAD
B84-AH REGULATOR VALVE ASSY-MARROTTA
VALVE CT

METEOROID PROTECTIVE ENCLOSURE DEPLOYED

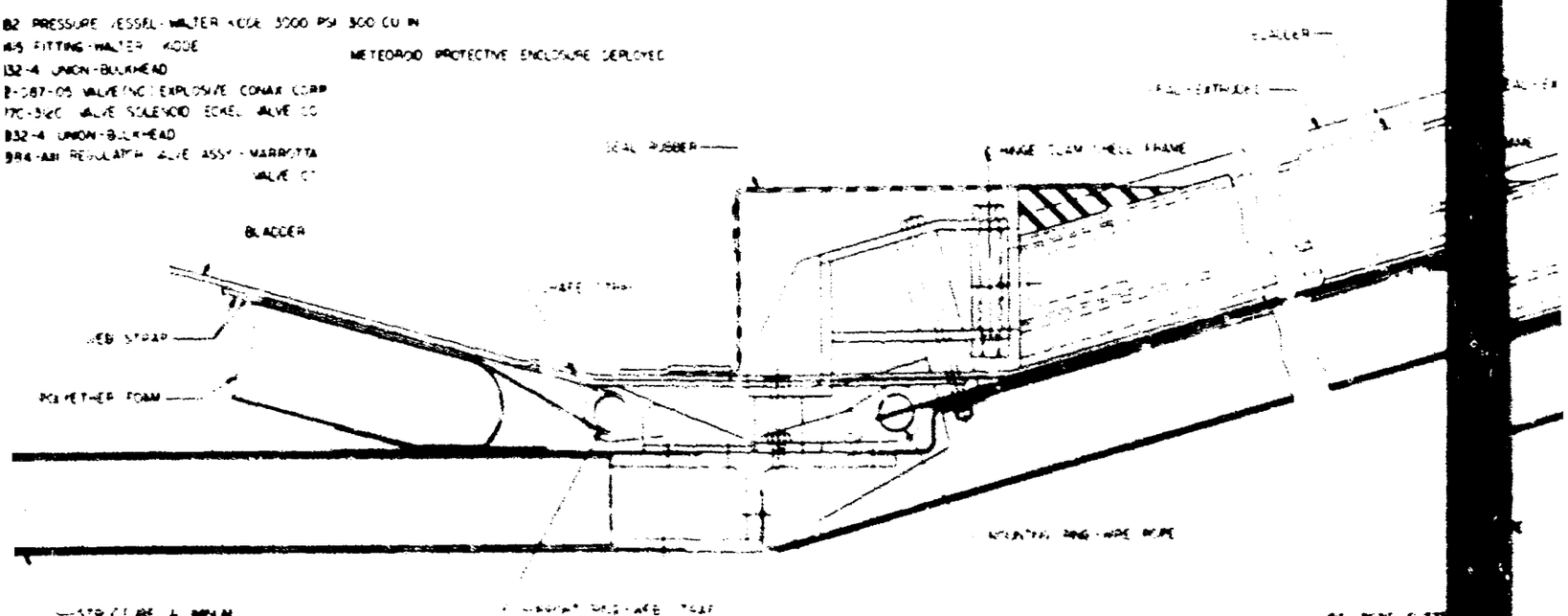

SECTION A-A
SCALE -

A

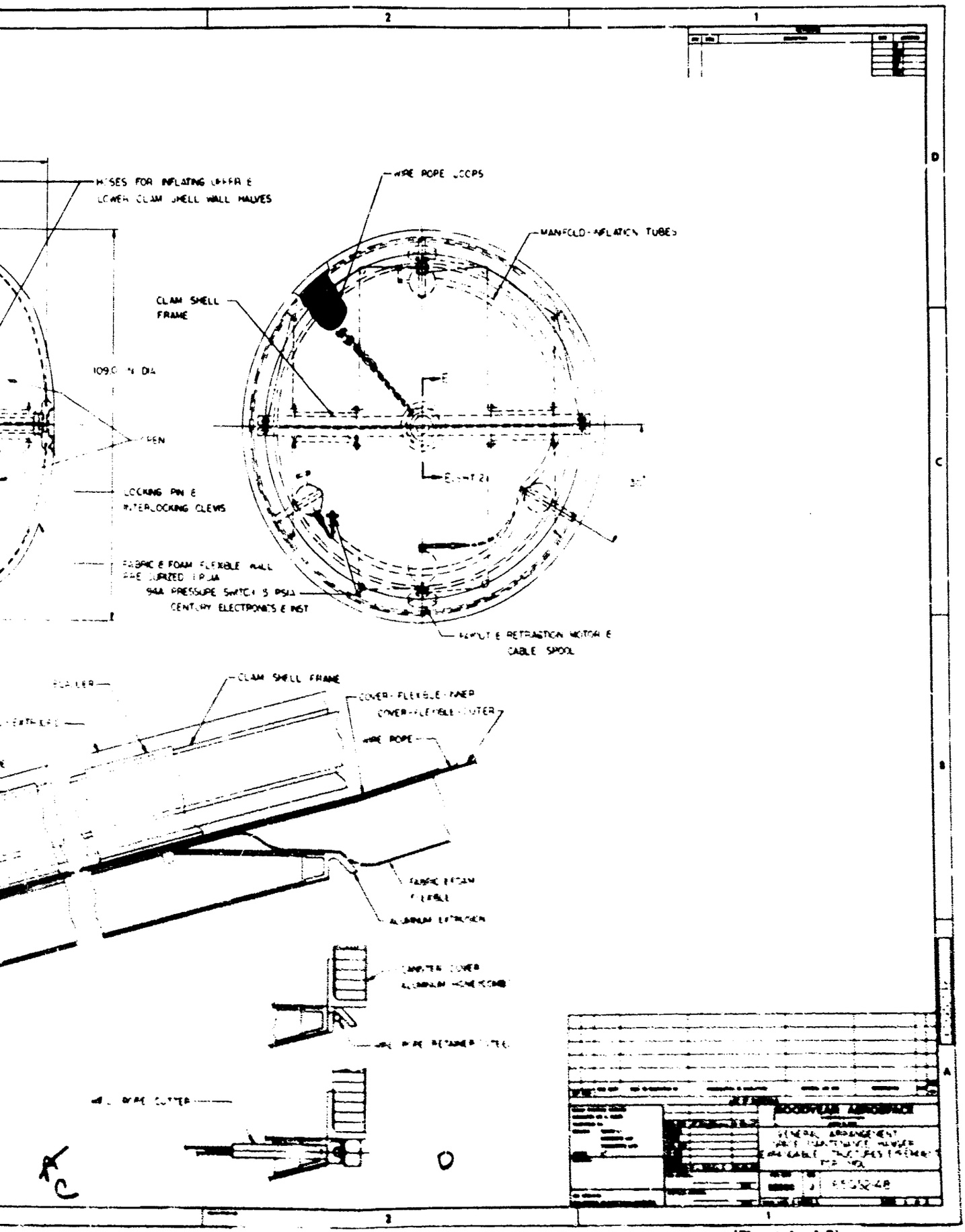

Figure 1. Space Maintenance Hangar, General Arrangement (Sheet 1 of 2)

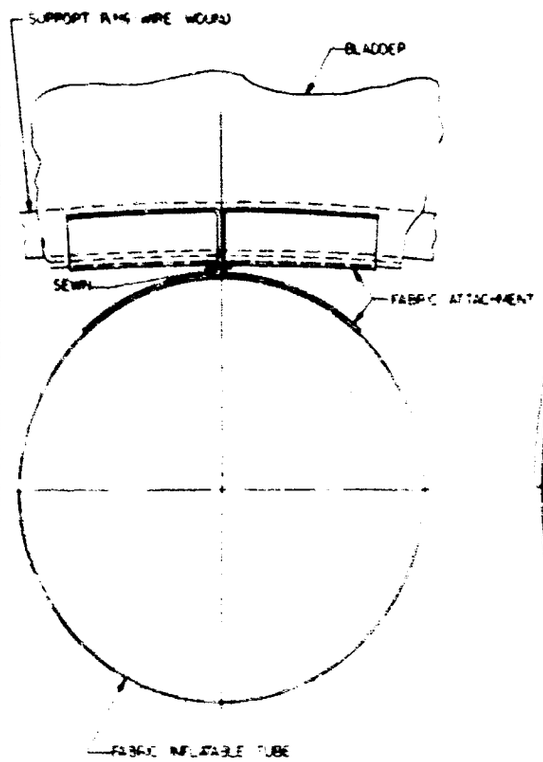

SECTION H-H (SHT)
SCALE

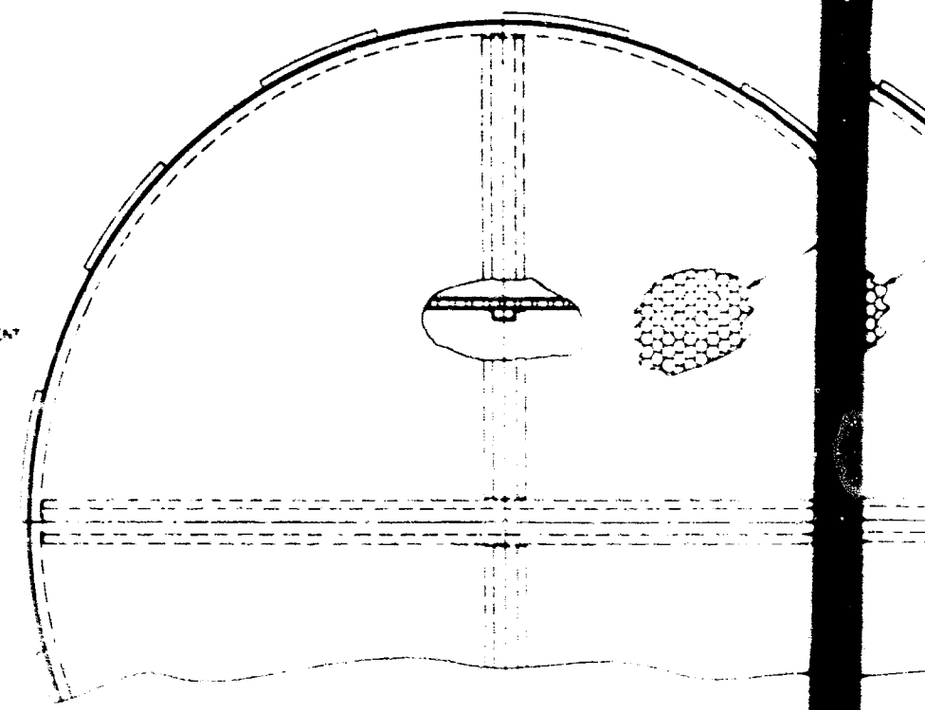

(SHT)
SCALE

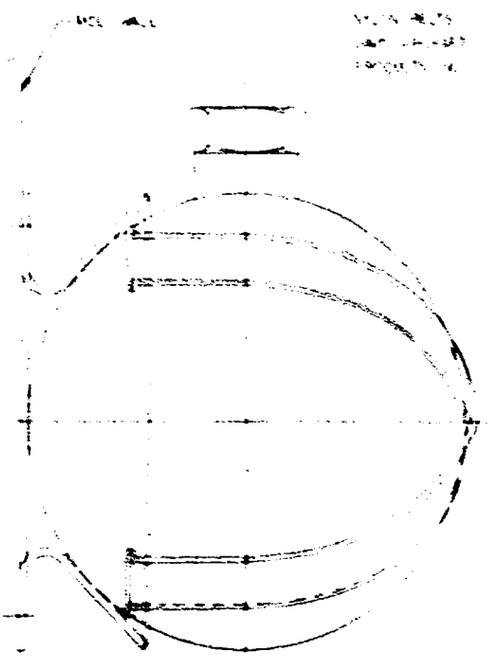

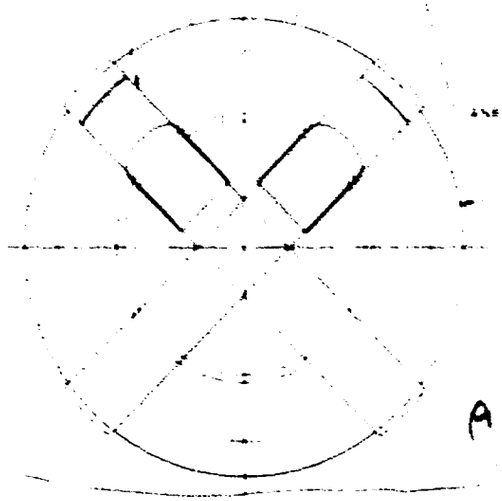

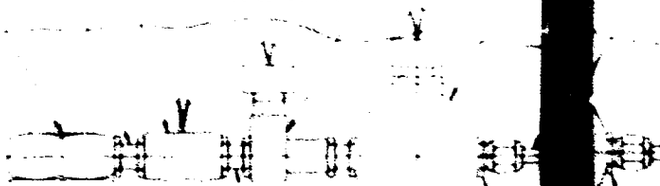

A

SECTION
SCALE

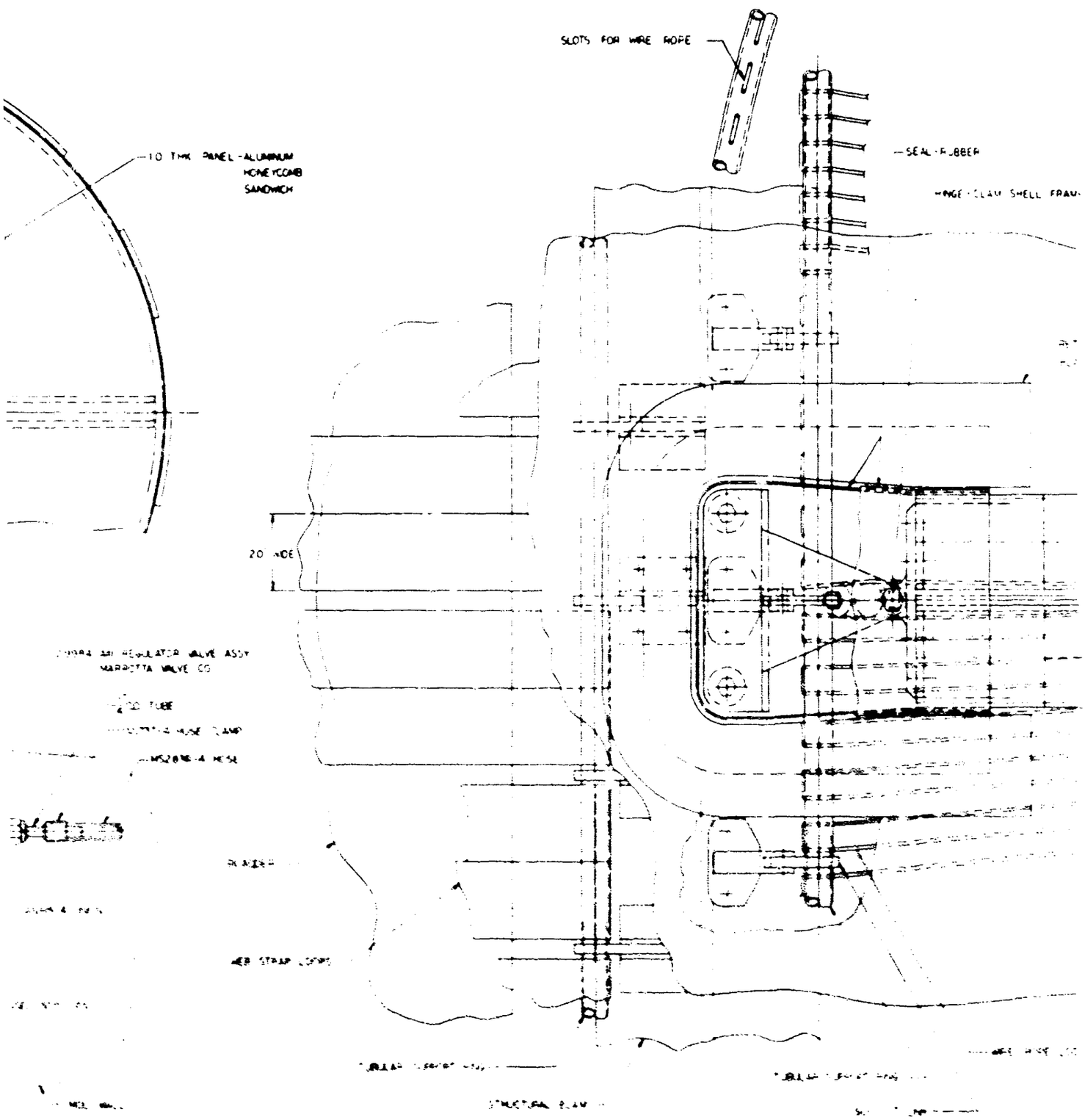
SLOTS FOR WIRE ROPE
SEAL - RUBBER
HINGE - CLAM SHELL FRAME

ER

CLAM SHELL FRAME

RETAINER - SEAL
BLADDER MATERIAL

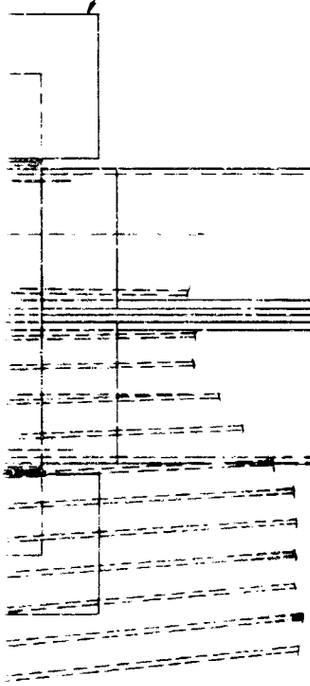

WIRE ROPE - LOOPED - CONTINUOUS

SECTION E-E (SHT 1)
SCALE 1

C

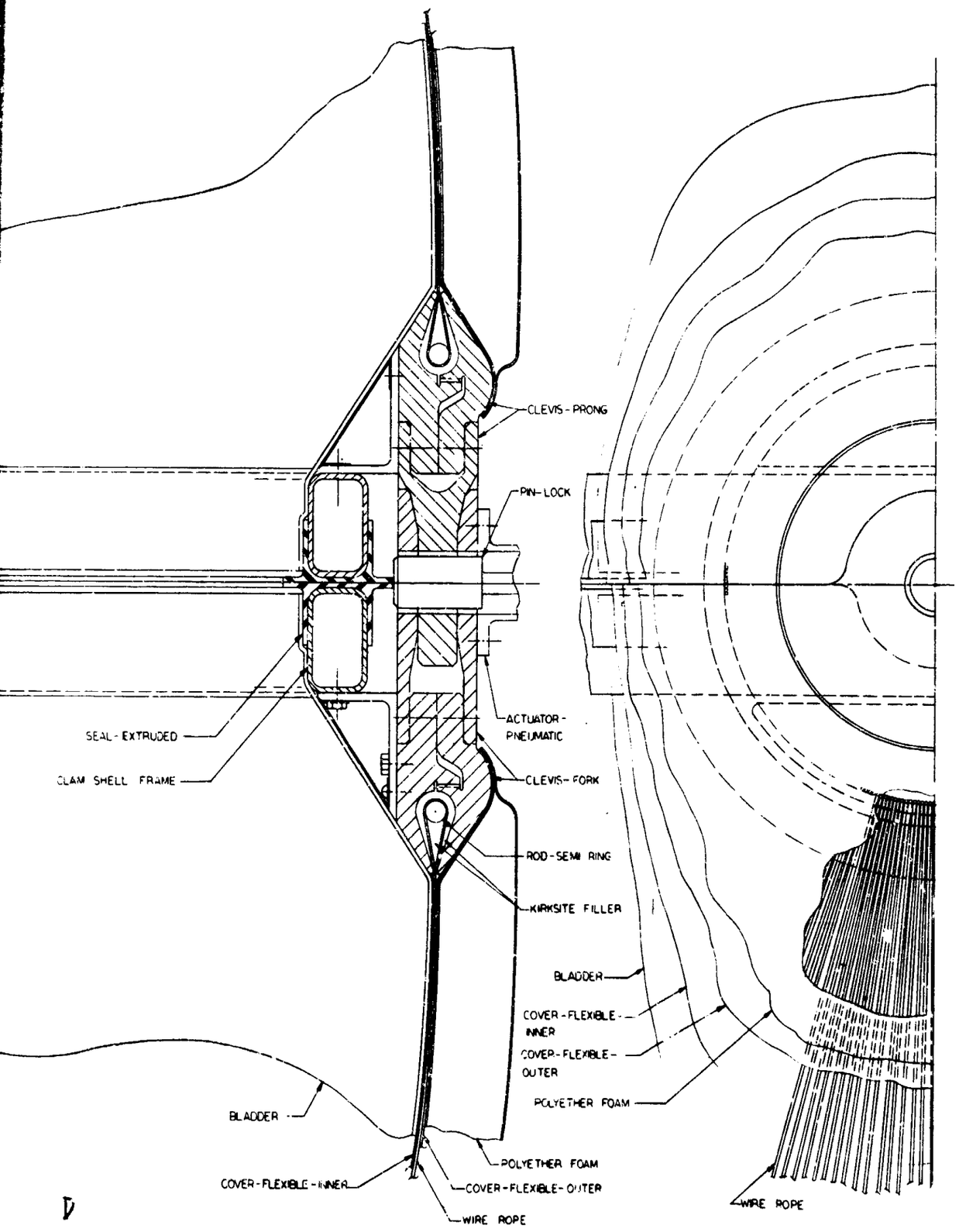

Figure 1. Space Maintenance Hangar, General A

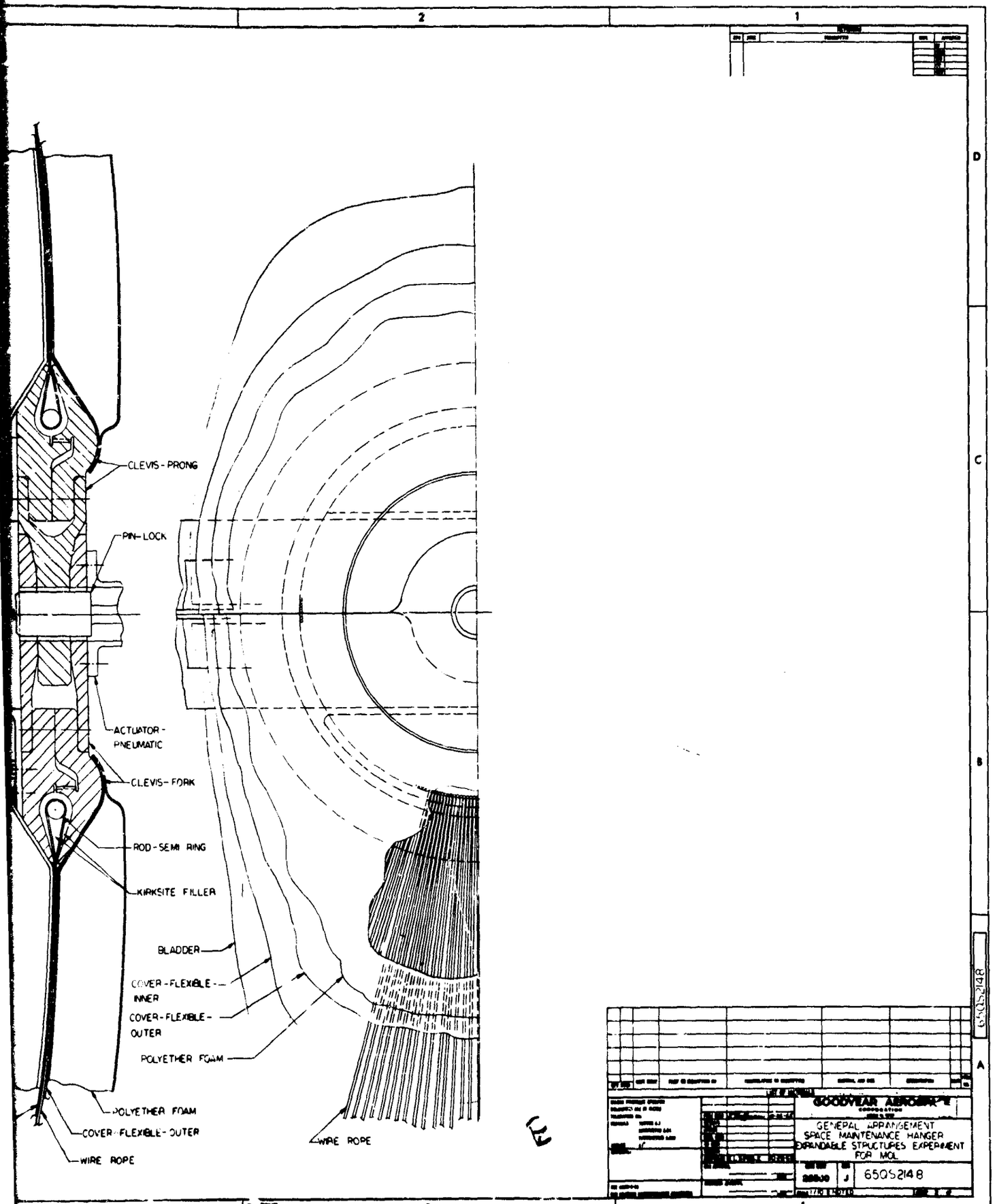

Figure 1. Space Maintenance Hangar, General Arrangement (Sheet 2 of 2)

SECTION III

CONCEPT DEFINITION

A. GENERAL

The concept definition portion of the program was limited arbitrarily to a one-month study. The objective of this phase was definition of the space maintenance hangar in conceptual form. Studies in each subsystem area were conducted within the constraints and requirements stated previously. The selection of a single concept was made before the subsequent initiation of the preliminary design and analysis. The results of the review and the approach taken is summarized in the following subsections.

B. INTERFACE DESIGN

The terminal end of the protective closure structure (attachment to the MOL) incorporates an aluminum base plate fastened to the head of the MOL. A steel tube ring and an angular ring for termination of the flexible structure and the bladder is attached and sealed to the base plate.

C. MATERIALS

A specific composite-materials approach, the subject of Goodyear Aerospace in-house development, was chosen for the expandable space hangar structure. A diagram of the composite arrangement and functions is shown in Figure 2. The cross section is basically four components, each serving a specific purpose. Each component emphasizes an essentially continuous construction for maximum structural reliability. The characteristics and functions of construction are given below.

1. Pressure Barrier

A triple-seal gas-pressure bladder is used for the space hangar structure design. Based on the company's in-house development, the measured permeability of the three-barrier composite bladder is 1.0×10^{-4} psf/day using oxygen at 5 psia as the test gas. A hole that will permit leakage through one barrier only doubles the already negligible permeability rate. For the wall construction employed, the measured permeability rate indicates a gas loss for the enclosure of about 50 cc/min at 5 psia.

2. Structural Wall

As indicated in Figure 2, a two-inch Dacron webbing used for the structural wall is a continuous strip running axially to the hangar, configured to carry the catenary plus the forward and aft loads. Coils of wire rings placed at approximately 2-1/4 foot intervals take the hoop tension.

3. Micrometeoroid Barrier

The selection of flexible polyether foam as a micrometeoroid barrier is based on hypervelocity particle impact tests conducted at the AFML at Wright-Patterson AFB. As a result of these tests (0.005 gram particles at 27,000 fps), it is concluded that a 2-inch thick, 1.2-pcf foam barrier is adequate with respect to penetration resistance. With this foam barrier, the protection exceeds a 0.995 probability of zero penetration for a 60-day period.

4. Outer Cover and Thermal Coating

A lightweight outer cover composed of a Nylon cloth-Capran film laminate (0.015-inch thick) is used with the inner cover to encapsulate the foam and permit the exhausting of air from the foam barrier prior to packaging. It also permits inflation to provide a pneumatic force for

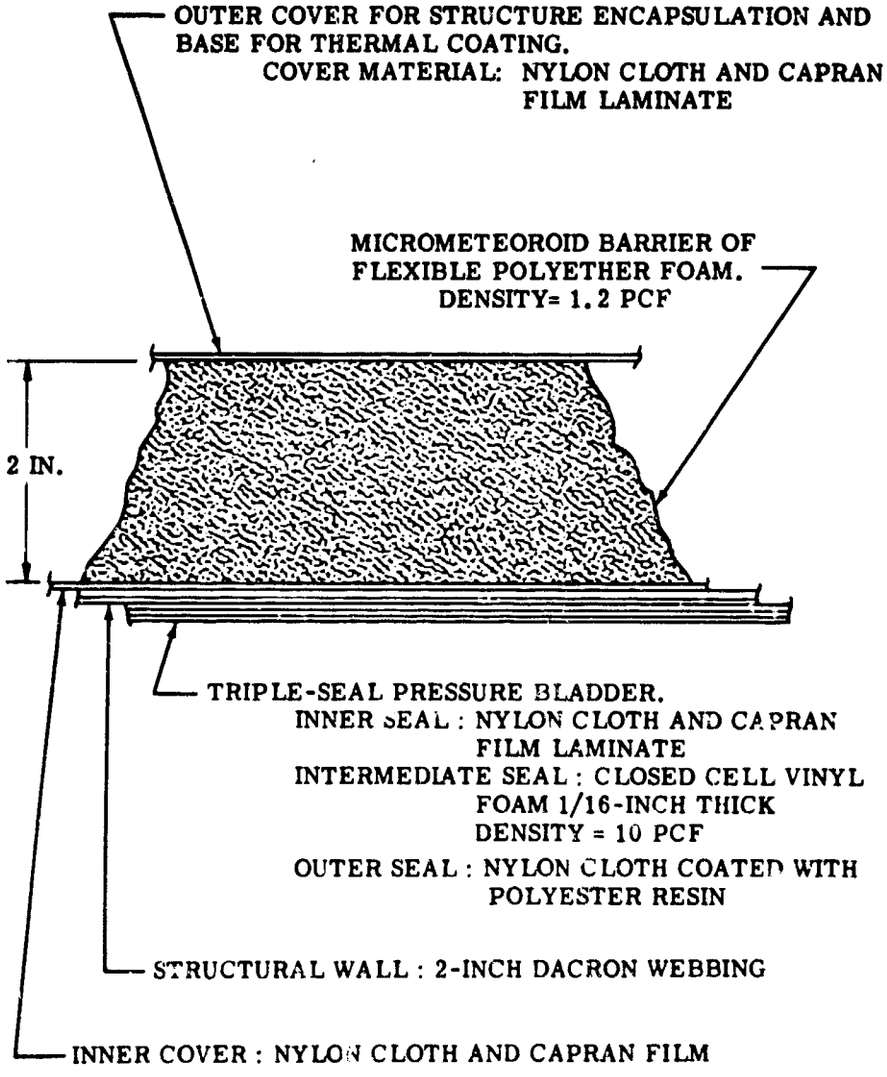

Figure 2. Composite Wall Cross Section

expansion of the foam on the end closure. All three thermal coatings considered satisfy the requirements. After better definition of the orbital characteristics, one of the three coatings will be applied to the outer cover surface to limit maximum surface temperatures and maintain a reasonable internal temperature.

D. PACKAGING AND DEPLOYMENT

In the concept, packaging and deployment are interrelated. For packaging the space maintenance hangar the 2-inch cylindrical wall is accordion-folded and stowed around the periphery of the cone structure. Due to the concept approach, only a packaging canister cover and a cylindrical adapter section are needed to complete the packaging requirements. The wall structure fold locations are controlled by radial rings positioned to provide a consistent folding pattern. All material (while in the stowed position) falls into a geometric pattern that facilitates deployment of the enclosure. Deployment of the garage is achieved by pressurizing the inflatable deployment tubes.

E. END CLOSURE

Although several approaches to the end closure design were reviewed, the mechanical clam shell concept, based on an isotensoid structural shape with zero hoop tension, was chosen. Structurally, this concept is predictable and reliable. Functionally, the doors are simple in construction and operation. Seals incorporated at the separation plane are those proven in other applications. The clam shell doors are closed and opened by an electric-powered reel and cable system which appears to be the most appropriate method.

SECTION IV

SPACE MAINTENANCE GARAGE STRUCTURE

A. GENERAL

The design and analysis effort covered a period of four months. The objective of this period was to establish feasibility of the selected concept approach through detail design of the system, supporting analysis, and specimen tests associated with full-scale hardware. The design effort translated the concept approach into a preliminary design drawing (Figure 1). The preliminary design is substantiated by supporting analyses which are described in the following sections. In addition, weight estimates of the final system design and a typical bay section are included.

For the selected concept, the space maintenance hangar is a combination flexible and rigid structure. It provides an habitable hangar for personnel and a protective enclosure for subsystems in a space environment. The total weight of the hangar is 1459 pounds with a usable volume of 900 ft^3. The enclosure is a 25-foot long accordion-pleated cylinder having a maximum diameter of 9.1 feet. The internal dimensions of the shelter measure 24.8 feet long with a minimum of 7.4 feet in diameter.

B. FLEXIBLE STRUCTURE

The flexible structure consists of a wall, hoop rings and an end closure. The cylindrical portion of the hangar utilizes a Dacron webbing structure composed of 244 longitudinal straps, unsupported in the circumferential direction. At approximately 2-1/4 foot spacing, a series of four large and four small hoop rings, in addition to the terminating rings, laced to the webbing complete the basic structure. The hoop rings of two different diameters, alternated, give the configuration its accordion shape in the unloaded condition. Under load, however, considering no stretch in the webbing, the straps take a catenary deflection which remains constant for the specified inner ring diameter and bay spacing. Because of this relationship, the maximum diameter of the flexible cylinder is dictated in the configuration.

Primary structural loads are carried axially by the webbing looped fore and aft on the terminating rings. Radially the loads are taken by the hoop rings spaced along the structure. Pressure loads are transmitted to the load carrying members by the gas-tight pressure bladder.

The basic structure measures approximately 20.5 feet long and 9.1 feet in diameter. The end closure adds 4.3 feet to the overall length of the complete structure.

1. Wall Construction

A major factor in determining the basic wall structural approach are the constraints imposed by the packaging and deployment of the hangar. In complying with these limitations, a flexible, packageable structure evolved employing a composite wall construction. The wall material for the cylindrical structure, as shown in Figure 2, is divided into four individual layers and described in the following paragraphs.

a. Pressure Bladder. The pressure bladder, bonded to the inner surface of the structural layer, serves as a gas barrier for pressure tightness. Its structural capability also permits bridging across a gap in case of the strap failure. The bladder, as shown in Figure 3, is a three-layer lamination of flexible sealant materials. The outer layer is a close-woven nylon cloth coated with polyester resin. The sandwiched layer is a 1/16-inch thickness of Vinyl foam and the inner layer is nylon film-cloth laminate. To facilitate construction, the pressure bladder is laid up on a 120 degree segment hangar mandrel. The inner laminate of cloth and film is applied first, followed by the layup of the foam-nylon cloth sub-assembly. Both

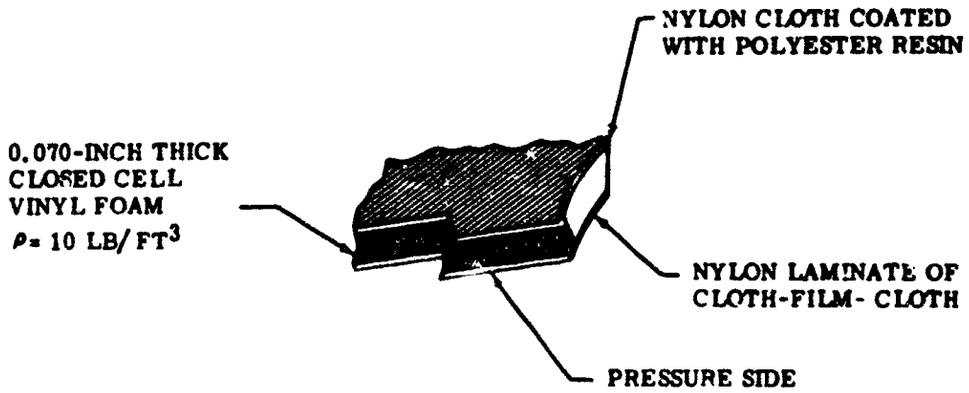

NOTES

(1) Construction - 3-Layer Laminate:

Inner Nylon Laminate	0.015 lb/ft^2
Polyester Adhesive	0.027 lb/ft^2
Closed-Cell Vinyl Foam	0.042 lb/ft^2
Polyester Adhesive	0.027 lb/ft^2
Outer Nylon Cover	0.015 lb/ft^2
	0.126 lb/ft^2

(2) Permeability

1.0 x 10^{-4} lb/ft^2 - Day at 5 psia
(Hangar Permeability = 0.06 lb/day)

(3) Toxicity

No Toxic Contaminants Detected

(4) Vacuum Test (10^{-6} mm Hg)

Off-Gassing	6.25 Percent Weight Loss
Stabilized (Approximate)	96 Hrs

Figure 3. Pressure Bladder

laminates are made with longitudinal panels equally spaced around the circumference of the mandrel arc. Seams for the individual layers have a 1-inch lap joint. The splice pattern for both subassembly laminates is staggered to prevent fabric build-up in local areas. The mandrel segment is rotated, as work progresses, to complete the circumferential lay-up.

b. Structural Wall. Upon completion of fabrication for the pressure bladder, the strap structure is incorporated. At a predetermined spacing, terminating rings for the webbing are positioned. Under nominal tension, to maintain a uniform strap length, a continuous strip of webbing is routed between the two rings, looping around the ring tubes to form a complete cycle. The 122 loops required to provide the structure are equally-spaced around the circumference of the rings. For added safety, in case of a strap failure, all loops are sewed, adjacent to the termination rings, with a sewing pattern capable of carrying the web break strength. This also eliminates the possibility of a cascading failure effect.

The following is a description of the Dacron webbing:

(1) Webbing Size	2.00 x 0.0114 inch
(2) Ultimate Tensile Load	675 lb
(3) Design Ultimate Load	665 lb
(4) Safety Factor	5
(5) Design Pressure	5 psi

c. Micrometeoroid Barrier. The foam barrier is provided to protect personnel, the structure, and interior components from micrometeoroids and thermal extremes. The barrier is a 2-inch thick flexible foam bonded to an inner cover. The polyether open-cell flexible foam barrier has a density of 1.2 pcf and weighs 0.20 lb/ft^2. The selection of flexible polyether foam as a micrometeoroid barrier is based on hypervelocity particle impact tests conducted at the AFML at Wright-Patterson AFB. As a result of these tests (0.005-gram particles at 27,000 ft/sec), it was concluded that foam of 1.2-pcf density is equivalent to single sheet aluminum of 15 times the mass per unit area. Thus, a 2-inch thickness of 1.2 pcf foam is considered equivalent to an aluminum sheet 0.53-cm thick (1.44 gm/cm^2) with respect to penetration resistance. Based on analysis, the probability of zero penetration for a 60-day period will exceed 0.995. The slabs of polyether foam are patterned and applied much the same as the vinyl foam for the bladder. In the cylindrical section, panels made of longitudinal straps are equally spaced around the circumference of the structure. The domed ends are tailored to match the contour. Panels are butt-spliced and bonded together at the edges to form a micrometeoroid barrier, an insulating shell and a protective spacer to alleviate excessive bends in the structural webbing during the packaged phase. The vacuum test (4.8 x 10^{-6} mm Hg) on the barrier material produced the following results:

(1) Off-gassing, 0.4 percent weight loss

(2) Stabilized in approximately 1.5 hr.

d. Cover. The inner and outer cover serve as a pressure barrier for the foam mat. The covers are bonded to the mat providing a pressure vessel of uniform thickness. The material and installation duplicate that of the inner laminate on the pressure bladder. Panels are also patterned in the same manner, providing for a one-inch lap splice. The basic difference between the inner laminate of the bladder and foam cover is the surface coating for temperature control on the outer cover. Although the cover serves primarily as a thermal barrier, it also functions as a protective surface for the foam and a pressure vessel for expanding the foam on the end closure. In addition, for possible packaging, the sealant laminate permits evacuation of the meteoroid barrier, thereby reducing the total wall thickness from approximately a 2-1/4 to a 3/4-inch thickness. The vacuum test (4 x 10^{-6} mm Hg) on the covers produced the following results:

(1) Off-gassing, 0.36 percent weight loss

(2) Stabilized in approximately 1.5 hr.

2. Hoop Rings

Four large and four small diameter rings in addition to the terminating rings carry the axial loads imposed on the cylindrical structure by internal pressure. The ring sizes are alternated and positioned along the cylinder at intervals of 25 and 28 inches; the typical unit bay section totaling 53 inches. In addition to carrying structural loads, the rings serve as spacers for the cylindrical straps and control for the folding pattern. By lacing the axial straps to the rings, the circumferential position is maintained during the stowed or packaged condition. The small diameter rings control the inner folds and the large rings determine the outside fold positions during packaging of the hangar.

As shown in Figure 1, the ring construction is made from coils of high-strength steel wire. The small rings with the larger loading conditions have 30 elements or coils and the larger ring contains 5 coils. The coils are bonded into a circular cross-section and are constrained with a wrapping of plastic-type tape. At installation, the rings are secured to the straps with linen cord applying the principles employed in lacing aircraft fabric to rib structure.

The following is a material description of the steel wire:

(1)	Wire diameter	0.080 inch
(2)	Ultimate Tensile Load	1382 lb
(3)	Design Ultimate Load	1382 lb
(4)	Safety Factor	3
(5)	Design Pressure	5 psi

3. End Closure

The dome-shaped end serves as the closure for the structure. The end is configured to a contour which provides zero hoop tension to simplify sealing along the closure frame and attendant structural problems. The geometry shown in Figure 4 (see Reference 1) is the contour approached by parachutes as the number of canopy lines are increased. The curve is rather flat, with the distance to the apex about 0.6 of the cylindrical radius.

The internal pressure in the end closure is carried by 480 equally-loaded meridian cables that terminate at the apex. Consequently a large force exists at the apex and causes a radial component to occur in the cable. This force is the product of the pressure and the area.

The meridian or radial cables are spaced at approximately 0.7-inch at the periphery of the rigid structure and converge at a 5-1/2-inch radius near the apex. Two clamshell frames hinged at the equator and located in the horizontal plane serve as the termination separation point for the pressure bladder. The frames control the domed end closure opening and provide support for the apex fitting and door pressure seal.

Except for the structural wall, the domed end wall construction duplicates that of the cylinder. Lay-up of the bladder is made on a segment of mandrel configured to the Taylor curve. The micrometeoroid barrier and covers are patterned to the appropriate contour. The wall structure differs from the cylinder in the following manner. At a predetermined distance, the terminating ring is positioned relative to the apex fitting. Under a nominal tension steel cables are threaded through the ring and looped at the apex. The 240 loops in the

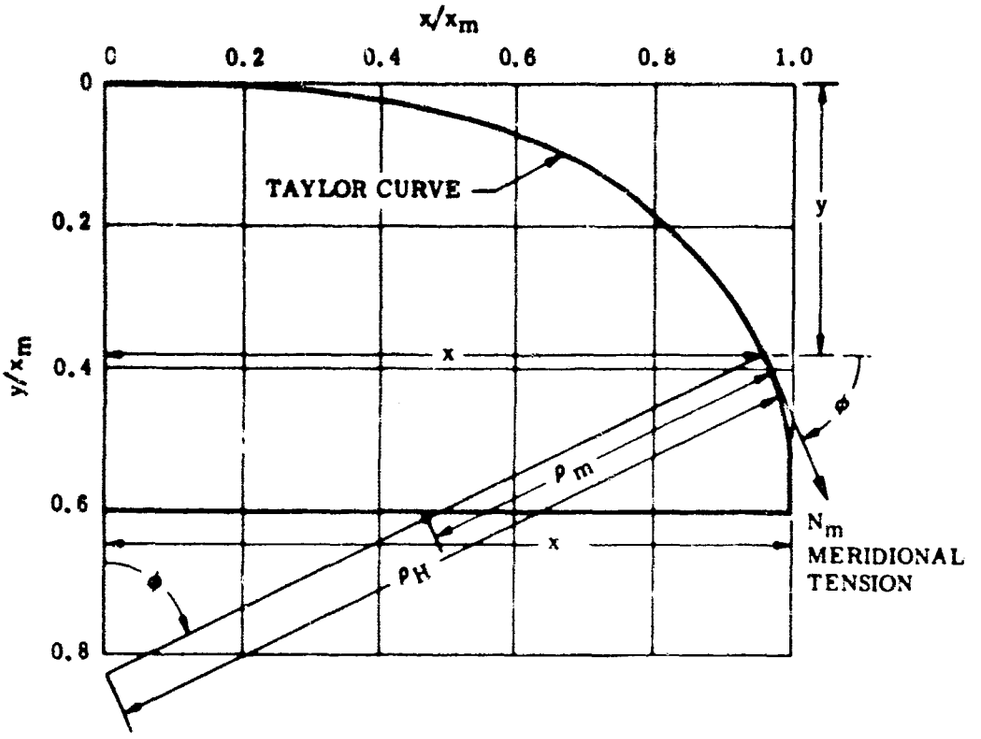

$$x = x_m \sqrt{\sin \phi}$$

$$y = \frac{x_m}{\sqrt{2}} \left\{ 2 \left[E\left(\frac{1}{\sqrt{2}}, \frac{\pi}{2}\right) - E\left(\frac{1}{\sqrt{2}}, \cos^{-1} \sqrt{\sin \phi}\right) \right] - \left[K\left(\frac{1}{\sqrt{2}}, \frac{\pi}{2}\right) - F\left(\frac{1}{\sqrt{2}}, \cos^{-1} \sqrt{\sin \phi}\right) \right] \right\}$$

F and E are elliptic integrals of the first and second kinds

K is a complete elliptic integral of the first kind

$N_m = \frac{px}{2 \sin \phi}$ where p is internal pressure

$N_H = 0$ (Not shown)

$\rho_H = \frac{x}{\sin \phi}$

$\rho_m = \frac{x_m}{2\sqrt{\sin \phi}} = \frac{1}{2} \rho_H$

Figure 4. Taylor Curve For Zero Hoop Tension

domed section provide the pressure structure for the enclosure end. The cables are equally spaced around the fitting and the circumference of the ring. For added safety, the cables embedded in Kirksite (at the apex fitting) secure the loops preventing slippage in case of a cable failure. Bonding of the bladder and foam cover to the stranded wire control the cable arrangement in the folded position.

The following is a description of the carbon steel wire rope:

(1) Cable size 7 x 7	0.067 inch dia
(2) Ultimate tension	480 lbs
(3) Safety factor	3
(4) Design pressure	5 psi

C. RIGID STRUCTURE

The rigid structure consists of a conical segment and a cylindrical adapter section with a box section compression ring joining the two at their interface. The conical segment is the aft portion of the shelter that, in conjunction with the compression ring, functions both as a support for the end enclosure and as the termination of the flexible cylinder aft end. The conical segment is also integral with the adapter section to form the packaging canister, thereby serving a dual purpose. The adapter section is attached to the MOL when the hangar is packaged and is separated from the MOL with electro-explosive frangible studs for deployment. In the packaged configuration, the smaller end of the conical segment is closed by an aluminum honeycomb sandwich canister cover. During the deployment sequence, before the clam shell doors are closed, the sandwich cover is released by cutting the wire retaining rope with electro-explosive cable cutters.

1. Conical Segment

The conical segment is the major assembly of the rigid structure. The overall size of the section is 109 inches in diameter at the interface with the cylindrical adapter tapering to 96 inches in diameter over a length of 25 inches.

The conical segment of the protective shelter consists of four basic items:

(1) The compression ring.

(2) Terminal ring attachments for both the cylindrical webbing and closure cables.

(3) Monocoque shell structure.

(4) Door frames.

Although the door frame is a part of the flexible dome structure, its construction is associated with the conical segment and therefore described in this section.

a. Compression Ring. The angle of intersection at the attachment of the flexible structure to the conical segment applies a compressive force on the circular cross section normal to the axis. This force is counteracted by a compression ring incorporated into the conical segment structure. The ring can be described as a box beam consisting of a heavy tee section and a heavy angle section. The base of the tee section forms the inner face of the ring and one leg of the angle forms the outer face of the ring with the leg of the tee and the other leg of the angle furnishing the vertical sides. In size, the diameter of the ring at the outer face is 109 inches. In cross section, the box beam is 3 inches wide and 2 inches deep. The tee section has a 5 inch base to provide for the attachment of the mounting ring for the closure cables.

Because of the circumferential length of the compression ring and the stretch forming required to contour the circular shape, the extrusion sections are spliced with butt welds and ground smooth. The compression ring is also used to partially support the hinge fittings that support the door frames.

b. Terminal Attachments. The flexible structure for both the cylindrical section and the domed end terminate at the conical segment in the area of the compression ring. The terminal tubes for these structures are located in planes perpendicular to the shelter longitudinal axis. Attachment points for these tubes occur at the inner face of the box beam. At these attachment points, heat-treated steel fitting are bolted to the tee section extrusion of the box beam. Steel support links provide a double shear connection between the strap termination tubes and the steel fittings.

c. Monocoque Shell Structure. The shell structure of the conical segment is a double wall skin and stringer monocoque structure. The largest end is attached to the compression ring, and the smallest end supports the canister cover retaining ring. The shell helps support the hinge fittings in conjunction with the compression ring, and supports the motors, and cable and reel system which opens and closes the clam-shell doors. The shell structure also serves as part of the packaging canister and guides the folds of the flexible doors when they are opened. The retaining ring has a notched flange arrangement which meshes with mating notches on the canister cover to support the wire rope retainer. The hollow spaces between the skins of the double wall shell are filled with foam similar to that used in the flexible structure so that the conical segment also provides a micrometeoroid barrier. The prime structural purpose of the conical shell, in addition to the support of the door cables from the point of tangency of the Taylor curve and the conic surface to the cable termination tube, is that of a pressure vessel to carry the inflation loads in the area between the tangency point and the compression ring. Since the shell is a surface of revolution, a conic surface, this task poses no problem as only tensile stresses are imposed on the skin.

d. Door Frame. The door frame consists of three basic parts as follows:

(1) The frame structure.

(2) The apex fitting.

(3) The pressure seal.

In relationship, the frame structures are joined with the hinge attachment which in turn is secured to the conical segment. The structures are also locked together with the apex fitting lock pin and sealed against leakage between the frames with an extruded seal system.

(1) Frame Structure. The clam shell frame structures for the shelter entry are basically box beams made from extruded channel butt welded and ground flush, centered on the equator of the conical segment and domed end. In planform, the box beams follow the slope of the cone and the Taylor curve. Construction of the two frames is similar with the only difference being in the hinge area. In cross section the box beam is 2-1/2 inches high and 1-1/2 inches wide. The thickness of the webs is 0.125-inch. The box beam cross section provides torsional rigidity. The frames are approximately 12-foot long from hinge fitting to hinge fitting. This length requires splicing the box beams at the apex by welding then grinding flush to maintain an uninterrupted seal surface. The hinge adapter fittings are extensions of the frames. Along the frame length, provisions are made for attaching the pulley brackets for the cable and reel door opening and closing system. In the center, brackets are incorporated to mount the apex fitting. The hinge attachment and door frames are installed as a unit. The attachment consists of a pin and hinge bracket coupled together. Fusing within the hinge joint is not anticipated because of the light loading condition.

(2) Apex Fitting. The apex fitting, discussed briefly in the flexible structure section (Section IVB), is located and supported at the center of the door frames. The fitting is essentially a clevis type arrangement with one-half of the fitting or cable terminal attached to

the upper frame and the other half supported by the lower structure. The assembled fitting measures 14 inches in diameter and 2-1/2 inches in width. The fitting, as shown in Figure 1, is made from heat-treated titanium material. The fitting is divided into four parts; two rings, fork, and prong. The rings transfer cable loads to the fork and prong. Each ring is made in one piece for ease in fabrication and assembly then threaded together to form an internally-tapered groove. This groove, undercut in cross section and located at the periphery of the ring, locks the flexible structure cables in position with Kirksite casting material. Through bearing, the Kirksite transfers the cable load to the ring. After the two rings are assembled into one piece, this is cut on a diameter into two equal pieces to be attached to each clam shell frame. Bolts thru one ring half and the fork, and thru the other ring half and the prong, transfer the cable loads from the rings to the fork and prong. Angular attachments adapt the apex terminal to the upper and lower door frames. The conical slope of the fork makes the two halves self centering. An end-tapered 1-1/4-inch diameter rod, activated by a pneumatic actuator, serves as the locking pin for the closure and transfers the cable loads from one side of the end closure to the other.

(3) Pressure Seal. The pressure seal for the closure is located between the upper and lower door frames. Grooves in the seals permit them to fit over the door frame box beams. As recommended by the B. F. Goodrich Company, Akron, Ohio, the seal follows the requirements of previous applications. The seal is made of silicone rubber and extruded in its collapsed position. In its collapsed position, the extended lips curve away from the attachment groove. In the expanded configuration, the overall cross-sectional dimensions are 2-3/4 by 1-1/2 inches. Closing the doors causes the tips of the curved extended lips to touch first; then further closing causes the lips to deflect and press against each other forming a gas tight joint. Pressurization causes the lips to press more tightly together. The mechanical properties of the section force the seal to return to its collapsed position when the internal pressure is released and the doors are opened. The design configuration of the clam shell door arrangement and the desired redundancy of the sealing provisions require the installation of two seal units.

2. Adapter Section

The adapter section is a monocoque structure canister that supports the launch inertia loading conditions on the packaged hangar. The adapter, attached to the base plate on the head of the MOL during launch, is configured to transfer these loads from the garage to the cylindrical structure of the vehicle. In shape, the section is cylindrical with a maximum diameter of 109 inches and a length of approximately 20 inches.

Except for attachment fittings, all material is aluminum alloy. The adapter is a double wall skin and stringer structure which is attached to the compression ring and is filled with foam to provide a micrometeoroid barrier for the flexible structure in the region of the compression ring where the longitudinal straps and flexible structure foam barrier terminate. Electro-explosive frangible studs are located around the periphery at the forward end to attach the adapter section to the base plate on the MOL during launch, and to separate the adapter section from the MOL for deployment.

D. WEIGHT BREAKDOWN

In conjunction with the drawing shown in Figure 1, the following is a summary of the weight analysis for the Space Maintenance Hangar:

Total Weight:		1459 pounds
Fabric Enclosure		715 pounds
Flexible Structure	489 pounds	
Thermal Coating	29 pounds	
Outer Cover	26	
Polyether Foam	143	
Inner Cover	27	

Lacing Strips	5 pounds		
Chafe Strips	5		
Web Straps	62		
Hoop Rings - Small	60		
Hoop Rings - Large	23		
Isotensoid Cables	22		
Tape	4		
Bladder	83		
Rigid Structure		125 pounds	
Tubular Support Rings	6 pounds		
Support Links	7		
Support Brackets	23		
Clam Shell Frames	28		
Spider	50		
Hinges	11		
Seals		38	
Actuator		29	
Miscellaneous		34	
Conical Segment			381 pounds
Compression Ring		116 pounds	
Skins		67	
Stiffeners		5	
Retaining Ring		16	
Canister Cover		122	
Wire Rope Retainer		2	
Reels and Cable System		25	
Foam		10	
Miscellaneous		18	
Cylindrical Adapter Section			76 pounds
Skins		46 pounds	
Stiffeners		9	
Separation Hardware		10	
Foam		7	
Miscellaneous		4	
Mounting Structure			168 pounds
Base Plate		133 pounds	
Support Ring		25	
Seals		2	
Miscellaneous		8	
Deployment System			49 pounds
Deployment Tubes		11 pounds	
Pressurization System		27	
Separation System		6	
Miscellaneous		5	
Miscellaneous			70 pounds

For use in expanding or shortening the shelter, a weight breakdown of a typical 53 incl. bay section is shown as follows:

Total Weight		100 pounds
Thermal Coating	5.5 pounds	
Outer Cover	5.1	
Polyether Foam	27.8	

Inner Cover	4.9 pounds
Lacing Strips	1.0
Chafe Strips	1.0
Web Straps	13.7
Cable Ring - Small	12.0
Cable Ring - Large	4.6
Tape	0.7
Bladder	14.6
Miscellaneous	9.1

SECTION V

MECHANICAL SUBSYSTEMS

A. GENERAL

Associated with the structural design of the Space Maintenance Hangar is the system design of the mechanical subsystems for operating the enclosure. These subsystems are primarily (1) the deployment system, (2) the door operating system, and (3) air pressure system. They are integrated to the extent that the enclosure will automatically deploy, the opening will open and close and the shelter will pressurize or deflate in the proper sequence. Although the studies of these subsystems have been carried through the preliminary design phase, the extent of detail does not parallel that of the structure. Figure 1 shows the mechanisms and the location of some basic components. Detail drawings, however, of mechanical parts, dependent on electrical power, the gas supply source, or mockup of the conceived designs for proof of operation, have not been considered.

B. DEPLOYMENT SYSTEM

Two modes of operation are used in the deployment system. For deployment, a pneumatic pressure provides the energy source for extending the deployment tubes. Pneumatic pressure also provides the energy source for assisting the expansion of the foam of the end closure.

The system for deploying the hangar consists basically of pressure vessels inflated with gas which in turn apply forces in the longitudinal direction to extend the enclosure mass. On the end closure, the meteoroid protection mat is designed as a pressure vessel. Gas barrier covers, sealed at the ends and bonded to the foam, contain the gas forced into the foam cavity. To expand the foam, pressures of 1/8 psi are anticipated, although provision is made for pressures as high as 1 psi.

The deployment system for the enclosure is shown in Figure 1. A gas line leading from the pressure source passes through an electro-explosive valve, a solenoid valve and a pressure regulator, to the deployment tubes. Initiation of deployment at the master control energizes an electro-explosive valve, normally closed, to the open position, permitting gas to flow through a solenoid valve and a pressure regulator into the deployment tubes. Forces applied to the tubes extend the cylinder until it reaches the required length. Pressure limit switches positioned in the deployment tubes close the solenoid valve, thereby terminating the deployment phase for the tubes.

C. DOOR OPERATING SYSTEM

Motor reels with a cable system close and open the clam shell doors. The system is shown in Figure 1.

1. Closing System

The clam shell doors are closed with one motor reel and two cable systems. Only the upper motor reel is used. Each cable extends from the reel over two pulleys mounted on the rigid conical segment and over one pulley mounted on the lower clam shell frame to a terminal on the upper clam shell frame. Reeling in the cables closes the doors. To maintain the doors in their closed position, the door structures are locked by a pin controlled with a pneumatic actuator. With a 100 psi system on the actuator, a force of 800 lbs engages the pin in the fork and prong of the apex fitting, and approximately 750 pounds is available for retracting the plunger. The foam on the end closure is pressurized by gas from the deployment tubes controlled by solenoid valves and pressure limit switches. Engagement of the two apex fitting halves at the termination of the closing operation contacts a limit switch. The limit switch

energizes three solenoids, opening valves to pressurize the foam mats. The latter function improves the thermal insulating quality of the foam and helps expand the foam which is tightly compressed by the closure folding to the packaged configuration.

2. Opening System

Referring to Figure 1, two reel units are shown positioned at the top and bottom of the conical segment near the compression ring. Four sets of cables run from the reels to pulley systems mounted in each quadrant of the conical segment and on the clam shell frames before returning to the reels. Each reel retracts the left and right hand quadrant cable installation and each torque motor is positioned for maintaining, if possible, equal and opposite forces to prevent destabilization of the conical segment. The door opening operation is initiated by a sequence timer after the hangar has been evacuated. Power to the solenoid valve pressurizes the actuator, pulling the pin from the apex fitting fork and prong. A limit switch in the pin retracted position energizes the two reel motors for opening the doors. The cable network prevents the flexible structure from dropping into the entrance opening. Limit switches on the lines disconnect the power when the door closure is fully open.

D. HANGAR PRESSURE SYSTEM

The enclosure cavity is pressurized to 5 psi from a supply source in the MOL. The system consists of a pressure reduction valve and solenoid. Pressure during use of the hangar is maintained through a reduction and energized solenoid valve. For depressurizing the hangar, the door frame seals become the means for evacuating the enclosure. The doors open until a limit switch indicates a 1/2-inch gap at the center of the door frame seals. In this position the gas escape area for the enclosure is equal to approximately 40 square inches. This method eliminates the need for solenoid exhaust valves. In addition, increased deflation time and increased system reliability are possible.

SECTION VI

MICROMETEOROID PROTECTION ANALYSIS

A. MICROMETEOROID ENVIRONMENT

The wall puncture hazard for micrometeoroids is assessed below in terms of the Poisson probability of no puncture. This probability depends upon the surface area, the exposure time and the flux of particles capable of puncturing the shelter wall. The perforation flux also depends upon the environment and the shielding effectiveness of the shelter wall.

In a near-earth orbit, the micrometeoroid environment is composed of both omnidirectional (sporadic) and unidirectional (shower) micrometeoroids. The following relationship (Reference 2) is accepted as the standard yearly average sporadic micrometeoroid environment:

$$\text{Log}_{10} N_{Sp} = -1.34 \log_{10} M - 10.423$$

where

N = number of impacts per square foot per day of particles Mass M or larger,

M = mass in grams.

A similar relationship can be written for the shower micrometeoroid environment in a near-earth space, i.e.

$$\text{Log}_{10} N_{Sh} = -1.34 \log_{10} M - 2.68 \log_{10} V + \log_{10} F - 6.465$$

where

V = geocentric velocity of the meteoroid stream (km sec.)
Averaging overall large showers per year gives an average velocity of 40 km/sec.,

F = ratio of accumulative meteor stream flux to the sporadic meteor flux.

The sporadic meteoroid flux is applied to the total surface area of the vehicle whereas the shower meteoroid flux is applied to only the average projected area of the vehicle. The space maintenance hangar in a near-earth orbit will be shielded during part of its orbit by the earth against both shower and sporadic micrometeoroids. This shielding (viewing loss) is given by the following expression:

$$L = \text{Viewing loss} = \left(1 - \frac{\sqrt{(R + H)^2 - R^2}}{R + H}\right) 2$$

where

R = radius of shielding body (earth),

H = altitude of orbit above the earth's surface.

The total number of micrometeoroid impacts (I_T) for particles of mass M or greater encountered by the garage can be given by the following equation:

$$I_T = (1 - L)(A_S N_{SP} + A_p N_{Sh})\tau$$

where:

A_S = surface area of the garage

A_p = average projected area of the garage

τ = mission duration

If the average velocity of all shower micrometeoroids is about 40 km/sec then a good approximation is that

$$N_{Sh} = F N_{Sp}$$

or

$$I_T = (1 - L) N_{Sp} (A_S + F_{Ap})\tau$$

B. MATERIAL SELECTION

To comply with the contractual specifications, a probability of zero penetrations greater than 0.995 is required. This requires that the protection material used on the shelter must be capable of stopping a certain minimum mass projectile M_m as can be seen from the Poisson probability of zero punctures (P_o) expression, i.e.

$$P_{(o)} = e^{-I_T}$$

$$= e^{-(1 - L) (A_S + F A_p)\tau N_{Sp}}$$

$$P_{(o)} = e^{-(1 - L) (A_S + F A_p)\tau 10^{-10.432} M_m^{-1.34}}$$

$$\left(M_m^{-1.34}\right)^{3/4} = \left[\frac{-\log_e P_{(o)}}{(1 - L) (A_S + F A_p)\tau \times 10^{-10.432}}\right]^{3/4}$$

$$M_m = \left[\frac{(1 - L) (A_S + F A_p)\tau \times 10^{-10.432}}{-\log_e P_{(o)}}\right]^{3/4}$$

Experimental and theoretical results indicate that depth of penetration of micrometeoroids into most materials is dependent on the 1/3 power of their mass. From past test experience on materials (References 3, 4, and 5) very similar to the proposed hangar material, GAC has shown that a 5 mg hypervelocity projectile will penetrate the structural wall when the low density foam is less than 1.5 inches and will cause no significant damage to the structural wall when the foam is 1.75 inches or thicker. Using the 1.75 inch thickness to stop a 5 mg projectile one obtains the following expression for penetration depth (T) as a function of projectile mass (M_m):

$$T = \left(\frac{M_m}{5 \text{ mg}}\right)^{1/3} \times 1.75 \text{ inch.}$$

Substituting M_m from the above expression that equation becomes:

$$T = \left[\frac{(1 - L) (A_S + F A_p)\tau \times 10^{-10.432}}{-\log_e P_{(o)}}\right]^{1/4} \times \frac{1.75 \text{ inch}}{(5 \times 10^{-3} \text{gms})^{1/3}}$$

For the space maintenance garage the appropriate parameters for the desired mission and vehicle are,

$1 - L \approx 0.7$ for 160 nmi orbit

$F = 1.0$

$A_g = 600\ ft^2$

$A_p = 230\ ft^2$

$\tau = 60$ days

$P_{(o)} > 0.995$

Upon substituting these parameters into the above equation the curve of Figure 5 is obtained.

To insure a 0.995 probability of no penetrations a foam thickness of about 1.6 inches is indicated. The above equations can be used to show that this probability of no penetrations, for the protective enclosure, requires that the material be capable of stopping particles which have a mass of about 3.8 mg. Experimental data on a similar material (Reference 4) indicates that a 5 mg projectile is adequately stopped by about 1.75 inches of foam. Therefore to assure a probability of no penetrations greater than 0.995, a foam thickness of 2.00 inches is considered quite sufficient.

Material for the polyether foam is described as follows:

(1)	Type	UU-15
(2)	Thickness	2.0 inch
(3)	Density	1.2 lb/ft^3

It should be noted that there is a continuous in-house effort on studies relative to protective materials for micrometeoroid environment. At present an approach under consideration employs a bumper wall (at least 15 mil) which is set away from the low density foam barrier. Basically, the concept reduces the foam thickness and installs a fabric curtain which is set at least an inch from the foam. Preliminary experimental results indicate that reduction of the foam thickness by about a factor of 2 is possible, thereby reducing weight. At the present time, Goodyear Aerospace has a company-funded project on this concept. More testing is to be dore in the near future.

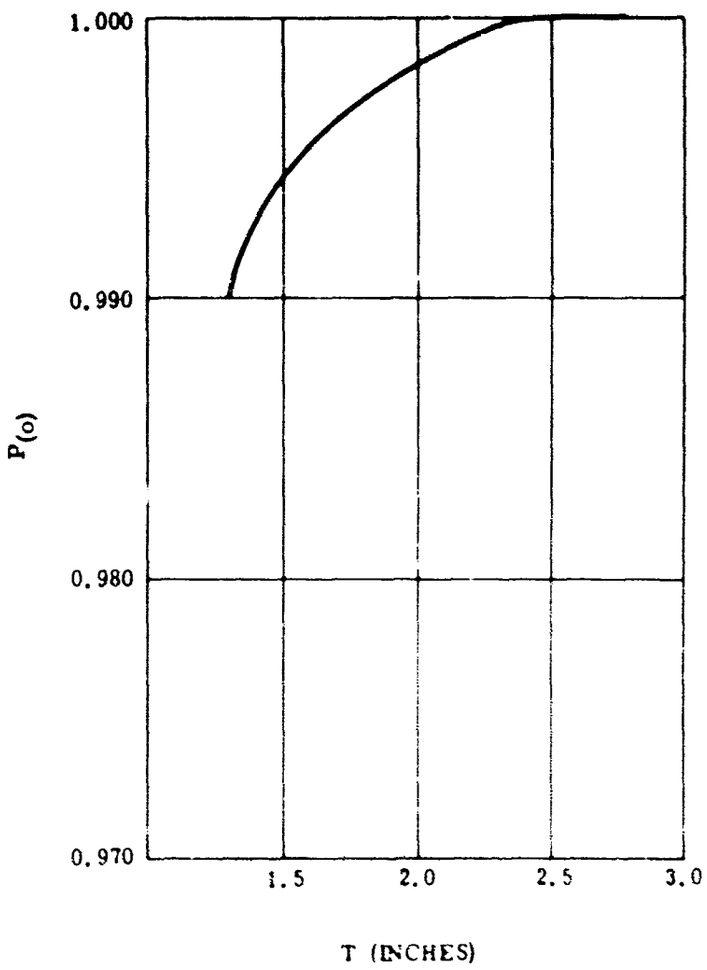

Figure 5. Probability of Zero Penetrations ($P_{(0)}$) Versus Foam Thickness (T)

SECTION VII

THERMAL CONTROL ANALYSIS

A. INTRODUCTION

The space maintenance hangar configuration analyzed in this section is that shown in Figure 1. For simplicity this configuration is regarded as a cylinder 8.2 feet in diameter with a hemispherical end and a total length of 24.8 feet. Two types of surfaces form the system: a double-wall aluminum conical segment which houses the expandable section in the collapsed position, and an inflated section covered by a micrometeoroid barrier discussed in a previous section.

Thermal design criteria are:

(1) A comfortable "room temperature" is to be maintained within the system for human habitation and reliable equipment operation.

(2) Material temperature limitations are not to be exceeded. Hot spots or cold spots may exist for brief periods on the external surfaces where the temperature limitations are approximately -300° F to 250° F.

(3) Internal system surfaces must be white to enhance lighting.

(4) The thermal design must be compatible with the project concept of a simple, erectable hangar.

Criteria (3) is easily satisfied by the use of white paint. A vehicle rotation of one rpm is presumed to alleviate the severity of the hot and cold spot problem, so that avoidance of certain hot (large ratio of solar absorptance to emittance) coatings will insure compliance with Criteria (2). Criterias (1) and (4) are somewhat contradictory. Thermal control coatings meet the above requirements. Due to weight and complexity, adjustable louvers and heat pumps with a radiator would seem to be excluded from consideration. Temperature variations are caused by the effects of variable internal heating, degradation of thermal coatings and insulations, and variations in external heating. The latter is caused by variations in earth albedo and reradiation intensities as well as orbital changes with respect to and as the earth progresses about the sun, and computational errors. Thermal coatings will assure adequate temperatures for equipment reliability and will permit human occupancy with the aid of protective clothing (shirt sleeves to winter clothing). In order to maintain a shirt-sleeve environment with a much tighter temperature band, a more sophisticated thermal control system will be required; the basic vehicle thermal control system may conceivably be used for this purpose.

This section presents the results of analyses to produce a tentative thermal design and illustrate the effect of various thermal parameters on the system temperatures.

B. TECHNICAL DISCUSSION

1. External Heat Flux

The Space Maintenance Hangar is heated externally by three types of thermal radiation:

(1) Solar radiation,

(2) Earth reflected solar radiation (albedo),

(3) Earth infrared reradiation.

The magnitude of these heating terms depends upon the type of orbit selected for the hangar. All orbits will lie between the two thermal extremes of a day-night orbit and a twilight orbit. A day-night orbit is defined as passing through the earth-sun line, and is possible with either an equatorial or polar launch. The twilight orbit is defined as one remaining over dawn and dusk areas of the earth, and is possible only with a polar launch. The thermal analysis will be limited to these two orbital extremes. The typical orbital altitude of 160 nautical miles specified for these studies is expressed in a dimensionless altitude term K defined as:

$$K = R_e/(R_e + h_o) \tag{1}$$

so that K = 0.96 for this application.

In order to obtain the albedo and earth radiation intensities upon the hangar the radiation view factors from the hangar to the earth will be required. Consider a flat surface with an orientation angle β with respect to the earth-surface line (β = 0 when surface faces earth). The view factor from the surface to the earth is then:

$$F_\beta = K^2 \cos\beta \qquad 0 \leq \beta \leq \cos^{-1} K$$

$$F_\beta = K^2 \cos\beta\left[1 - \sin^{-1}(f_1/K \sin\beta)/\pi\right] + \left[\sin^{-1}(f_1/\sin\beta) - f_1 f_2\right]/\pi \qquad \cos^{-1} K \leq \beta \leq \pi/2$$

$$F_\beta = \left[K^2 \cos\beta \sin^{-1}(f_1/K \sin\beta) + \sin^{-1}(f_1/\sin\beta) + f_1 \right. \qquad \leq \beta \leq \cos^{-1}(-K)$$

$$F_\beta = 0 \qquad \cos^{-1}(-K) \leq \beta \leq \pi \tag{2}$$

where

$$f_1 = \sqrt{K^2 - \cos^2\beta}$$

$$f_2 = \sqrt{1 - K^2}$$

Equation (2) is plotted in Figure 6. The view factor from the cylindrical portion of the hangar to the earth is:

$$F_c = \int_0^{\pi} F_\beta \, d\beta = \int_0^{\pi} d\beta \tag{3}$$

Equation (3) is integrated numerically to obtain a value of F_c = 0.38277. The view factor from the hemispherical portion of the hangar to the earth is the same as that from a sphere to the earth which is:

$$F_h = 0.5(1 - f_2) \tag{4}$$

so that F_h equals 0.36 for this application. The value of the view factor from portions of the hemisphere to the earth vary, of course, from $F_e = F_{z=2}$ = 0.32410 on the equator to 0.38277 where the hemisphere merges into the cylinder, with the 0.36 being an average value.

Earth reradiation flux intensity on the hangar is independent of the type of orbit. Taking the value of the earth albedo (a) as 0.36 and the solar constant (C) as 442.4 Btu/hr-ft^2,

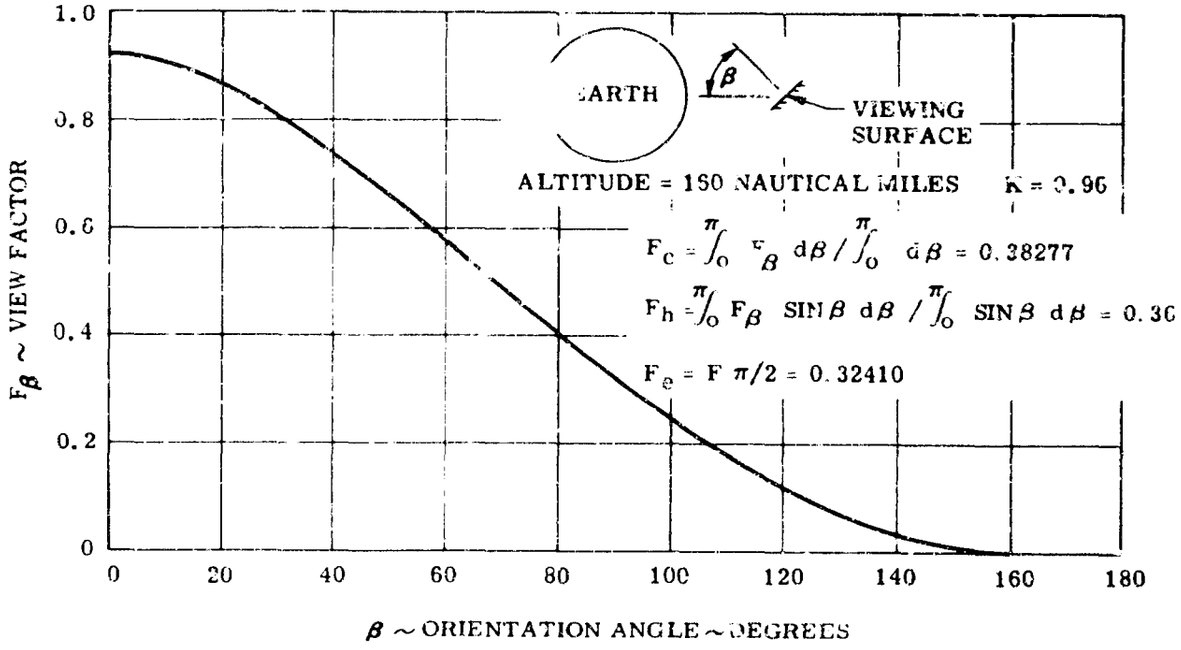

Figure 6. Radiation View Factor of Earth

$$E_c = C \frac{(1 - a)}{4} F_c = 27.09$$

$$E_h = C \frac{(1 - a)}{4} F_h = 25.48$$

$$E_e = C \frac{(1 - a)}{4} F_e = 22.94 \qquad (5)$$

Solar and albedo intensities vary with the type of orbit. For a day-night orbit let θ be the orbital angle measured from the earth sun line in the direction of flight. The hangar is then in the umbra for values of θ between 105^o and 255^o.

Since the hangar follows the attached vehicle the solar fluxes are:

$$S_{c,\theta} = C (\cos \theta) \text{ abs}/\pi \qquad 255^o \leqslant \theta \leqslant 105^o$$

$$S_{c,\theta} = 0 \qquad 105^o < \theta < 255^o$$

$$S_{h,\theta} = C (1 + \sin \theta)/4 \qquad 270^o \leqslant \theta \leqslant 105^o$$

$$S_{h,\theta} = 0 \qquad 105^o < \theta < 270^o$$

$$S_{e,\theta} = C \sin \delta \qquad 0^o \leqslant \theta \leqslant 105^o$$

$$S_{e,\theta} = 0 \qquad 105^o < \theta < 0^o \qquad (6)$$

Orbital average values are:

$$S_c = \int_0^{2\pi} S_{c,\theta}\, d\theta / \int_0^{2\pi} d\theta = 46.35$$

$$S_h = \int_0^{2\pi} S_{h,\theta}\, d\theta / \int_0^{2\pi} d\theta = 64.52$$

$$S_e = \int_0^{2\pi} S_{e,\theta}\, d\theta / \int_0^{2\pi} d\theta = 88.63 \qquad (7)$$

Considering the low orbital altitude, the albedo fluxes are reasonably approximated as:

$$Q_{c,\theta} = C\, a\, F_c \cos \theta \qquad 270^o \leqslant \theta \leqslant 90^o$$

$$Q_{c,\theta} = 0 \qquad 90^o < \theta < 270^o$$

$$Q_{h,\theta} = C\, a\, F_h \cos \theta \qquad 270^o \leqslant \theta \leqslant 90^o$$

$$Q_{h,\theta} = 0 \qquad 90^o < \theta < 270^o$$

$$Q_{e,\theta} = C\, a\, F_e \cos \theta \qquad 270^o \leqslant \theta \leqslant 90^o$$

$$Q_{e,\theta} = 0 \qquad 90^o < \theta < 270^o \qquad (8)$$

Orbital average values are:

$$Q_c = \int_0^{2\pi} Q_{c,\theta}\, d\theta \Big/ \int_0^{2\pi} d\theta = 19.40$$

$$Q_h = \int_0^{2\pi} Q_{h,\theta}\, d\theta \Big/ \int_0^{2\pi} d\theta = 18.25$$

$$Q_e = \int_0^{2\pi} Q_{e,\theta}\, d\theta \Big/ \int_0^{2\pi} d\theta = 16.43 \qquad (9)$$

For a twilight orbit the solar and albedo fluxes are constant:

$$S_c = C/\pi = 140.82$$

$$S_h = C/4 = 110.60$$

$$S_e = Q_c = Q_h = Q_e = 0 \qquad (10)$$

Average fluxes over the hangar may be obtained by treating the hangar surface area as 83.6 percent cylindrical and 16.4 percent hemispherical end, then:

$$E_g = 0.836\, E_c + 0.164\, E_h = 26.83 \qquad (11)$$

For a day-night orbit:

$$S_g = 0.836\, S_c + 0.164\, S_h = 49.33$$

$$Q_g = 0.836\, Q_c + 0.164\, Q_h = 19.21 \qquad (12)$$

For a twilight orbit:

$$S_g = 0.836\, S_c + 0.164\, S_h = 135.86$$

$$Q_g = 0 \qquad (13)$$

2. Equilibrium Temperatures

The external heat fluxes previously derived may be used to compute the radiation equilibrium temperatures of the hangar external surfaces as well as the internal temperature. Neglecting internal heating and internal heat transfer, a heat balance on any surface takes the form:

$$\epsilon \sigma T^4 = E\epsilon + (S + Q)\, \alpha$$

or

$$\sigma T^4 = E + (S + Q)\, \alpha/\epsilon \qquad (14)$$

The equilibrium temperature is seen to be a function of the external heat fluxes and the ratio of solar absorptance (α) to emittance or infrared absorptance (ϵ). Utilizing the fluxes of Equations (5, 7, and 9 through 13), the resultant temperatures are plotted in Figure 7 as a function of the α/ϵ ratio.

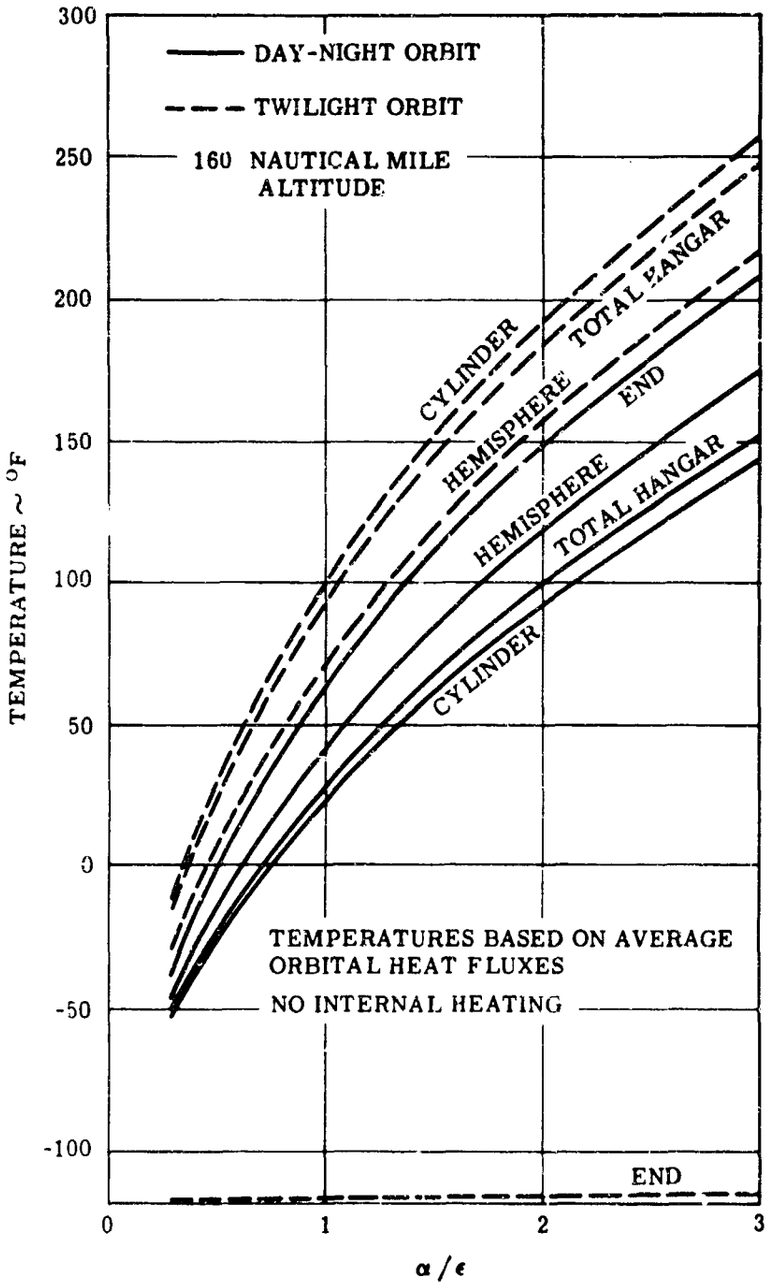

Figure 7. Space Maintenance Hangar Equilibrium Temperatures

It may be observed from Figure 7 that:

(1) An average α/ϵ ratio near 1.5 appears desirable for a day-night orbit, while a ratio near 0.75 appears desirable for a twilight orbit.

(2) The type of orbit makes a difference in temperature of approximately 70°F.

(3) Local temperatures on the hangar surface, other than the tip or end of the hemisphere, vary by only about 20°F. It may be noted that the end surface comprises a very small percentage of the total hangar area.

The Figure 7 temperatures will, of course, rise if internal heating occurs. Internal heat transfer will dampen the local temperature variations. Since the heat fluxes utilized are averages, the temperatures are averages about which the actual temperatures will cycle as the hangar rotates and moves around the earth.

3. Rotational Transient Temperatures

As the hangar rotates at the presumed rate of one rpm, the external surface will experience variable heating which will cause temperatures cycling at the rate of one cycle per minute. This effect is most severe on the inflated surface of the hangar, as opposed to the conical segment, since the inflated surfaces have less mass and are better insulated from the interior surfaces. For this reason the inflated cylindrical surfaces are selected for a study of the transient temperatures of the hangar.

Before a transient analysis can be accomplished, a thermal model of the affected surfaces must be constructed. The inflated surfaces have two primary components, a pressure bladder and a micrometeoroid barrier. Two concepts of micrometeoroid barriers have been used to construct two thermal models as shown in Figure 8. Since the polyether foam acts as thermal insulation, the pressure bladder is insulated from the transient temperature variations, closely follows internal temperatures, and is presumed to have a constant and typical temperature of 75° F. Thermal conductivity of the open cell polyether foam is an important parameter which is variable; the conductivity is approximately 0.24 Btu-in/hr-ft^2-$^{\circ}$F initially but, following penetration of the outer laminate by micrometeoroids, outgassing will eliminate gaseous conduction across the cells and reduce this conductivity to approximately 0.07 Btu-in/hr-ft^2-$^{\circ}$F (Reference 3). The latter value produces the most severe transients and is used in the transient studies. Each model is arbitrarily divided into five nodes as shown in Figure 8, and the slight surface curvature is neglected.

A heat balance on each node of the 2-inch model may be written:

$$\frac{K_t}{y}(T_2 - T_1) + (S + Q)\,\alpha + E\epsilon = \epsilon\sigma T_1^4 + (\omega c_p)_1 \frac{dT_1}{d\tau}$$

$$\frac{K_t}{y}(T_{i+1} + T_{i-1} - 2T_i) = (\omega c_p)_i \frac{dT_i}{d\tau}, \qquad 2 \leqslant i \leqslant 5 \qquad (15)$$

where y is the distance between nodes, T_6 is defined as 75° F (534.7°F), and $(\omega c_p)_i$ is the thermal mass of node i. For the 1-inch model:

$$(S + Q)\,\alpha + E\epsilon + \epsilon_I \sigma T_2^4 = (\epsilon + \epsilon_I)\sigma T_1^4 + (\omega c_p)_1 \frac{dT_1}{d\tau}$$

$$\frac{K_t}{y}(T_3 - T_2) + \epsilon_I \sigma T_1^4 = \epsilon_I \sigma T_2^4 + (\omega c_p)_2 \frac{dT_2}{d\tau}$$

$$\frac{K_t}{y}(T_{i+1} + T_{i-1} - 2T_i) = (\omega c_p)_i \frac{dT_i}{d\tau}, \qquad 3 \leqslant i \leqslant 5 \qquad (16)$$

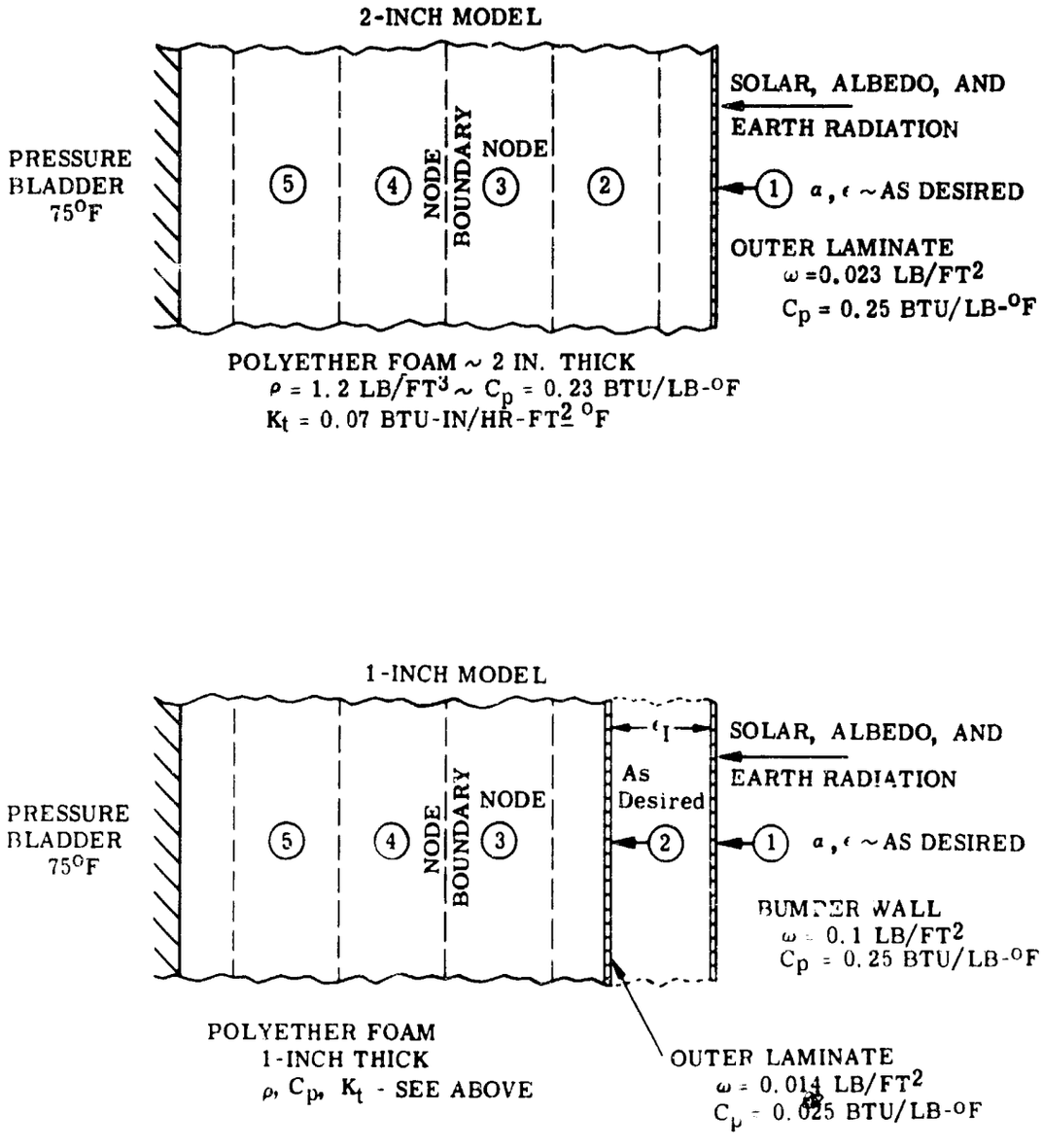

Figure 8. Thermal Models of Inflated Surface for Transient Studies

where ϵ_I is the effective emittance between nodes 1 and 2 defined as:

$$\epsilon_I = (\frac{1}{\epsilon_1} + \frac{1}{\epsilon_2} - 1)^{-1} \tag{17}$$

The external heating terms must be evaluated as a function of time (τ). A somewhat conservative and greatly simplified analysis of rotational response results if the cylindrical surface is presumed normal to sunlight while albedo and earth radiation are neglected; with a one rpm rotation:

$$S = C \cos(120\,\pi\,\tau) \qquad 270^0 \leqslant 120 \leqslant 90^0$$

$$S = 0 \qquad 90^0 < 120 < 270^0$$

$$Q = E = 0. \tag{18}$$

Utilizing equation (18), equations (16) and (17) are solved numerically, by a backward difference technique, to obtain transient equilibrium solutions (cyclic repetitive temperatures). Values of the variables α, ϵ, and ϵ_I must be specified as input data. Figure 9 presents the results of this study. A black surface ($\alpha = \epsilon = 0.9$) produces transient temperature differentials of 96° F on the surface of the 2-inch model, approximately 45°F on the bumper of the 1-inch model, and 0.4°F to 12°F respectively on the outer laminate surface of the 1-inch model for values of ϵ_I from 0.025 (aluminized Mylar, or similar substrate, surfaces) to 0.8 (black or high ϵ white surfaces). Lower values of α and ϵ will decrease these differentials as well as transient temperatures resulting from a day-night orbit. State-of-the-art coatings which appear desirable for hangar application are:

(1) Aluminized Mylar or similar substrate. Typical properties are $\alpha = 0.15$, $\epsilon = 0.05$, $\alpha/\epsilon = 3$.

(2) A thin layer of SiO on aluminized Mylar. Typical properties are $\alpha = 0.15$, $\epsilon = 0.5$, $\alpha/\epsilon = 0.3$.

(3) Aluminized silicone white paint. Typical properties are $\alpha = \epsilon = 0.25$, $\alpha/\epsilon = 1$.

These three coatings may be combined by painting stripes or other patterns of coating (3) on sections of (1) or (2) to yield average values of from 0.3 to 3. The differentials produced by these coatings are observed from Figure 9 to be less than 28° F for the surface of the 2-inch model, 13° F for the bumper of the 1-inch model, and 4° F for the outer laminate surface of the 1-inch model. These rotational transient temperature variations must be considered when evaluating hot spot material temperatures, but have negligible effect on internal and system balance temperatures.

4. Hot Spot Temperatures

The polyether foam effectively insulates the outer laminate from the pressure bladder and hangar interior. It is conceivable that portions of the external surface may achieve local hot temperatures beyond material limitations even though the hangar interior is at a comfortable room temperature. Excessively cold temperatures, on the other hand, do not present a problem since the low orbital altitude and hangar rotation insure temperatures higher than minus 120°F. The high-temperature limitations of the polyether foam, outer laminate, and bumper wall may preclude or restrict the use of certain thermal coatings for these external surfaces.

For a twilight orbit the average surface temperature will not exceed those of Figure 7, with transient variations as the hangar rotates per Figure 9. The cylindrical surface is the warmest, but an α/ϵ ratio as high as 2 appears to cause no high temperature problem presuming material limitations in the order of 225°F to 250°F. Since the desired average α/ϵ ratio for internal temperature control is less than 1, limiting the α/ϵ ratio to a maximum of 1 will insure reasonable hot spot temperatures.

WHITE PAINT ($\alpha = \epsilon = 0.25$) ON ALUMINIZED MYLAR
($\alpha = 0.15$, $\epsilon = 0.05$) OR SiO ON ALUMINIZED MYLAR
($\alpha = 0.15$, $\epsilon = 0.50$)

POLYETHER FOAM CONDUCTIVITY = 0.07 BTU-IN/HR-FT^2-$^\circ$F

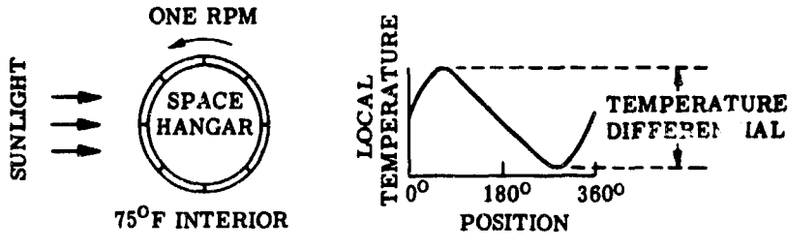

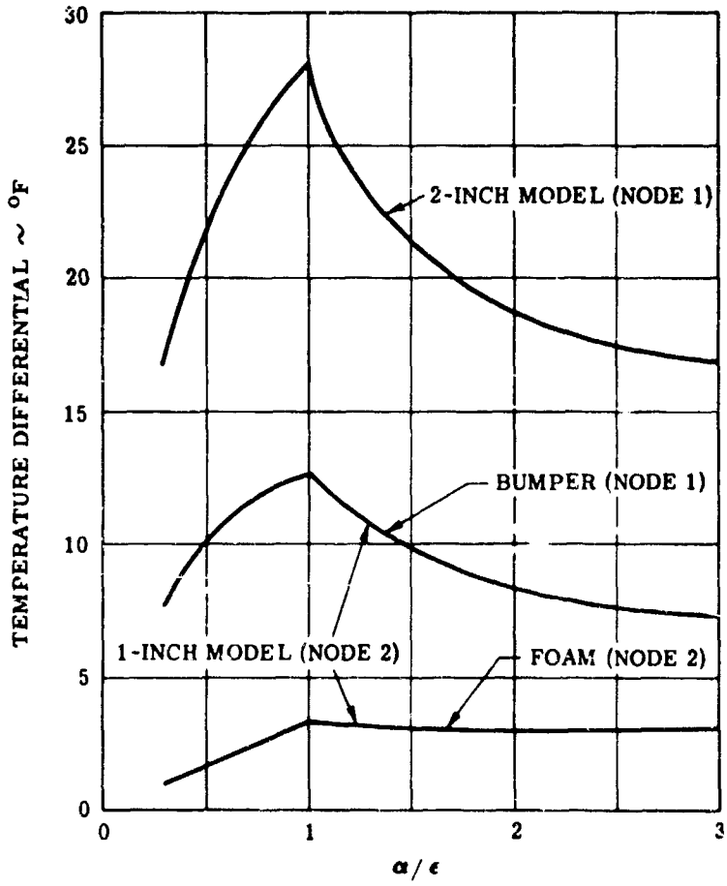

FOR $\alpha = \epsilon = 0.9$:
TEMP DIFF ON 2-INCH MODEL = 96 °F
TEMP DIFF ON 1-INCH MODEL :

BUMPER	FOAM	EFFECTIVE ϵ BETWEEN BUMPER AND FOAM
44.4 °F	11.6 °F	0.8
46.0 °F	0.4 °F	0.025

Figure 9. Rotational Response Characteristics of External Surface

For a day-night orbit the average surface temperatures are again given by Figure 7, but with transient variations not only as the hangar rotates but as the hangar passes through the day-night cycle. The latter effect is appreciable. To evaluate these transients the thermal models described by equations (15) and (16) are again utilized. Heat fluxes from earth reradiation, solar radiation, and albedo radiation were previously derived and presented in equations (5), (6) and (8) respectively as a function of the orbital angle θ. Since the orbital period is 90 minutes (1.5 hr), the orbital angle (θ) is related to time (τ) by the expression:

$$\theta = \frac{4}{3}\pi\tau \qquad (19)$$

The resultant transient equations are again solved numerically, utilizing a backward difference method, after specifying values for α, ϵ, and ϵ_I.

Results for the day-night orbit are presented in Figure 10 for the three low value α and ϵ coatings previously discussed. The end surface of the hemisphere is seen to be considerably warmer than the cylindrical surface. An α/ϵ ratio of 1 ($\alpha = \epsilon = 0.25$) appears to be the maximum permissible for the end surface, which does not encounter rotational transients. The maximum permissible α/ϵ ratio for the cylindrical surface appears to be 3. Since the average α/ϵ ratio desired for internal temperature control is greater than 1, it is obvious that the hemispherical end will require a different thermal coating than the cylindrical section. For comparison, use of a black coating ($\alpha = \epsilon = 0.9$) would produce cylindrical hot spot temperatures of 140° F on both models and end surface hot spot temperatures of 255°F on both models. Using an effective internal emittance (ϵ_I) of 0.025 rather than 0.3 with the $\alpha = \epsilon = 0.25$ coating on the 1-inch model increases the maximum bumper temperature to 132°F and 238°F and decreases the maximum foam temperature to 86°F and 120°F for the cylindrical and end surfaces respectively.

C. THERMAL DESIGN CONCLUSIONS

1. Variables Affecting Temperatures.

Temperatures within the hangar are affected by many variables or uncertainties, such as:

(1) Variable internal heating, variable external heating due to local variations in earth albedo and infrared reradiation as well as variations in the time spent in sunlight as the earth progresses about the sun.

(2) Uncertainties and degradation of thermal coating properties.

(3) Variation of polyether foam conductivity due to outgassing.

(4) Air circulation rate [illegible] the hangar.

(5) Computational [illegible]

Achievement of a [illegible] environment within the hangar with its narrow temperature band would requi[illegible] the thermal control system of the basic vehicle, or a fairly sophisticated hangar [illegible]rol system which would be inconsistent with the concept of a simple, erectable sh[illegible]rmal control coatings will, however, maintain internal temperatures at a level c[illegible] with reliable equipment operation, and suitable for human habitation with protective [illegible]g. A typical temperature band within the hangar may be 25°F to 100°F. Variations i[illegible]rnal temperature as the hangar passes through the day-night cycle may be approximately ±10°F, although the external surface temperature variation may be approximately ±150°F.

2. Selection of Optimum Thermal Coatings.

Selection of the optimum combination of external surface thermal coatings depends upon the following:

ALUMINIZED SILICONE WHITE PAINT ($\alpha = \epsilon = 0.25$) ON ALUMINIZED MYLAR ($\alpha = 0.15$, $\epsilon = 0.05$) OR Si O ON ALUMINIZED MYLAR ($\alpha = 0.15$, $\epsilon = 0.5$)
EFFECTIVE EMITTANCE BETWEEN BUMPER AND FOAM ON 1-INCH MODEL IS 0.8
POLYETHER FOAM CONDUCTIVITY = 0.07 BTU-IN/HR - FT^2 - ^oF

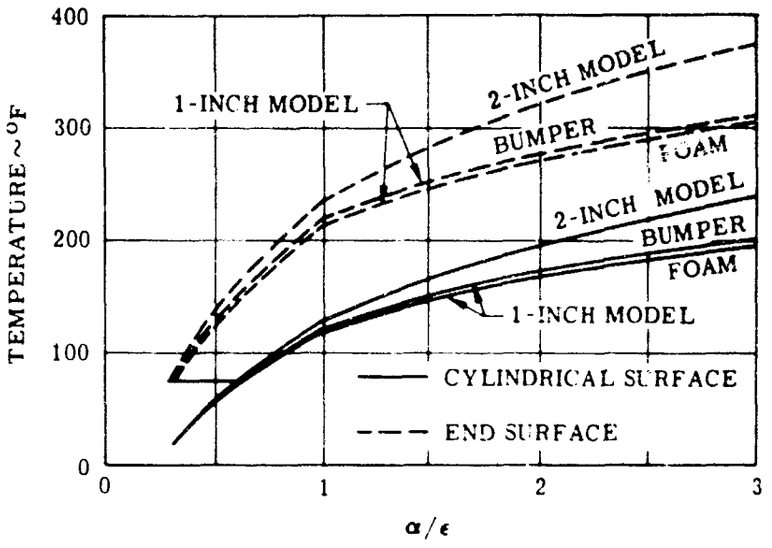

TYPICAL SURFACE TEMPERATURE VS TIME

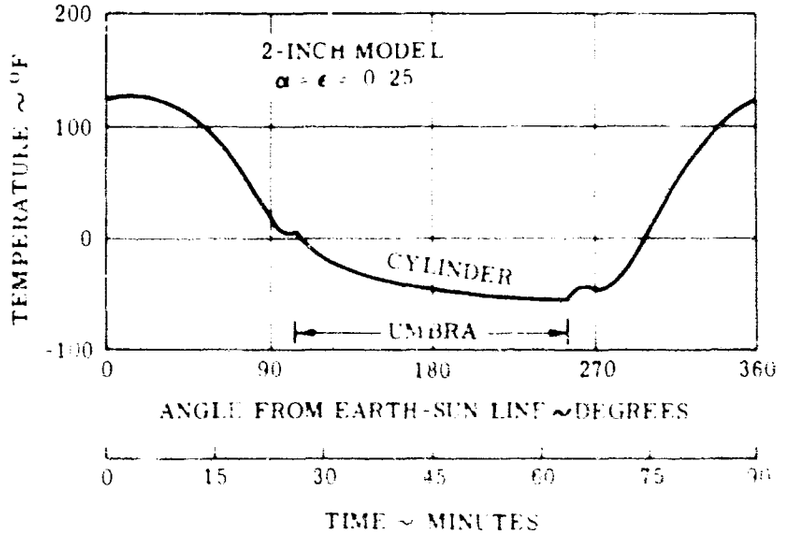

Figure 10. Maximum Temperatures In Day-Night Orbit - 75° F Interior

(1) Type of micrometeoroid protection system.

(2) Orbital inclination with respect to the ecliptic

(3) The internal temperature desired

(4) Considerations involving the attached vehicle thermal control system if utilized for hangar thermal control.

The optimum coating properties generally will not correspond to a single coating, and may require the combination of 2 or more coatings by striping or other means.

Preferred thermal control coatings for the inflated section external surface are:

(1) Aluminized Mylar (or similar substrate)

(2) SiO on aluminized Mylar

(3) Aluminized silicone white paint

Preferred for the conical segment external surfaces are zinc oxide pigmented methyl silicone elastomer white paint, black paint, and bare metal. All internal surfaces and the interfaces between the double wall of the conical segment should be covered with the zinc oxide pigmented white paint. Black paint is also acceptable for the interfaces. Redefinition of the optimizing condition may alter the combination of coatings required, but not the coatings. Different coatings are generally required on the cylindrical and end portions of the inflated structure and conical segment due to variations in local heat fluxes. The variations cause local hot spot temperature problems which can be alleviated by judicious selection of thermal coatings.

All thermal coatings described are currently state of the art with the possible exception of the aluminized silicone white paint, which has not been proven for inflated structures. Since the elastomer base is similar to that of the proven zinc oxide pigmented paint, no difficulties are anticipated.

3. Model Selection

The choice of micrometeoroid protection systems will probably be made on criteria other than thermal. Either selection is acceptable thermally. A slight preference is shown for the 1-inch system due to its versatility. With a zinc oxide pigmented white paint or black on the outer laminate and bumper wall interfaces, this model is less affected by internal heating. With reflective coatings on the interfaces, this model thermally resembles the 2-inch model.

It is recommended that this analysis be refined in the development and design stage of subsequent hangar contracts, utilizing information which should then be available on internal heat loads, required personnel environments, and orbital launch data obtained by the use of this study and mission analyses. Development and testing of the aluminized silicone white paint on inflated surfaces should be accomplished at the earliest opportunity.

SECTION VIII

STRUCTURAL ANALYSIS

A. GENERAL

Structurally the hangar consists of three primary components:

(1) Cylinder. Composed of longitudinal fabric straps and high strength steel wire cable hoops.

(2) Isotensoid End Closure. Having only meridional stresses carried by flexible carbon steel cables.

(3) Conical Frustum. Connects the cylinder and end closure.

In addition to the connections required for the primary structural components, a fabric bladder, a clam shell frame that facilitates opening of the end closure, and a split ring at the apex of the end closure required for termination of the meridian cables also must be considered.

For this preliminary design phase, the structure has been analyzed for internal pressurization only. No external loadings such as angular accelerations, docking forces, etc., have been considered. For the design, only the internal operating pressure of 5 psi and a proof test pressure of 10 psi were considered. This structural analysis is based upon the two loading conditions.

The factors of safety applied to the 5 psi pressure loading are 3 for the metal and 5 for the fabric components. Therefore, the corresponding factors of safety for the 10 psi proof pressure become 1.5 for metal and 2.5 for fabric components.

B. ISOTENSOID END CLOSURE

The inflated end closure, or dome, is designed as an isotensoid surface of revolution. These surfaces are used extensively in the filament winding of pressure vessels, rocket cases, etc. High strength-to-weight ratios result since a nearly uniform factor of safety is achieved throughout the body due to the constant stresses in the filaments.

In the problem at hand, the particular isotensoid surface chosen is that generated by a meridian curve of the equation, using coordinates as shown in Sketch (A),

$$x = x_t \sqrt{\sin \phi} \tag{20}$$

Commonly referred to as Taylor's curve, the equation provides constant tension in the meridional structural elements and also yields zero circumferential stresses everywhere. This may be shown by summarizing the original proof as given in Reference 1. Taking equilibrium on the element, $x dz$, $\csc \phi\, dx$, as shown in Sketch (B).

Forces normal to the axis of rotational symmetry lead to

$$\frac{d}{dx}\left(f_m x \cos \phi\right) = \frac{f_c}{\cos \phi} - p x \tan \phi \tag{21}$$

Forces parallel to the axis of symmetry lead to

$$\frac{d}{dx}\left(f_m x \sin \phi\right) = px \tag{22}$$

Sketch (A)

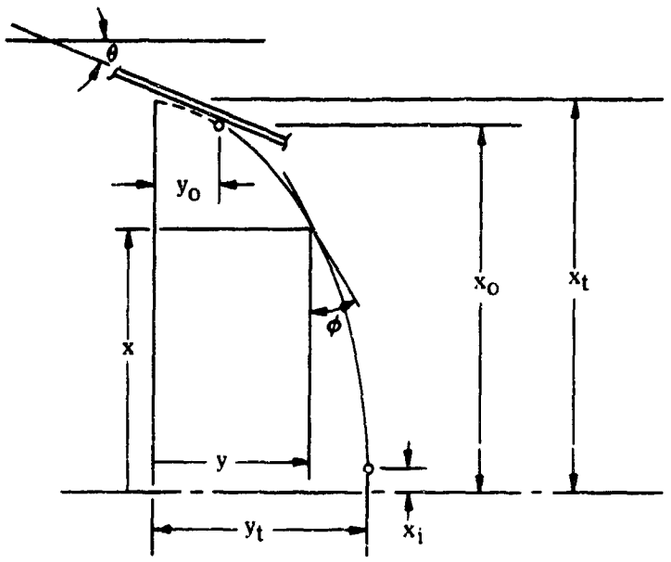

Sketch (B)

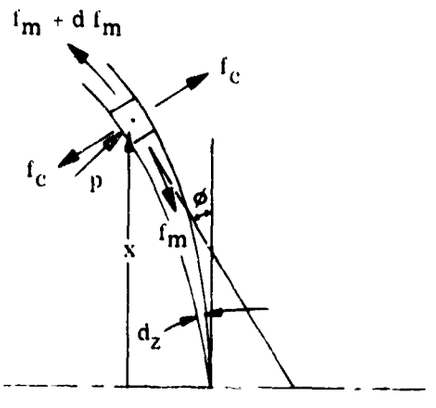

AXIS OF SYMMETRY

Operating on the left-hand sides of Equations (21) and (22) facilitates writing them in the form,

$$f_m x \frac{d \cos \phi}{dx} + \cos \phi \frac{d (f_m x)}{dx} = \frac{f_c}{\cos \phi} - px \tan \phi \tag{23}$$

$$f_m x \frac{d \sin \phi}{dx} + \sin \phi \frac{d (f_m x)}{dx} = px \tag{24}$$

Multiplying Equation (23) by $\cos \phi$ and Equation (24) by $\sin \phi$ and then adding gives,

$$\frac{d}{dx} (f_m x) = f_c \tag{25}$$

If f_c is now stipulated to be zero, from Equation (25), it follows that,

$$f_m x = \text{Constant} \tag{26}$$

Integrating Equation (22) and from Equation (26), yields the condition,

$$\frac{px^2}{2 \sin \phi} = \text{Constant} \tag{27}$$

Finally from the boundary condition, when $x = x_t$, $\phi = \pi/2$, the equation of the Taylor's curve is obtained,

$$\frac{px^2}{2 \sin \phi} = \frac{px_t^2}{2}$$

$$x = x_t \sqrt{\sin \phi}$$

An alternate approach to show that $f_c = 0$ is to use two equations; one considering the dome as a whole and taking static equilibrium parallel to its axis and the other is the well-known membrane equation (Reference 6).

Static equilibrium parallel to the axis of symmetry gives

$$2\pi x f_m \sin \phi = p \pi x^2$$

$$f_m = \frac{px}{2 \sin \phi} \tag{28}$$

The membrane equation is

$$\frac{f_m}{\rho_m} + \frac{f_c}{\rho_c} = p, \tag{29}$$

where ρ_m and ρ_c are the meridional and circumferential principal radii of curvature respectively and are derived from geometry as

$$\rho_m = \frac{ds}{d\phi} = \frac{dx}{\cos \phi \, d\phi} = \frac{1}{\cos \phi} \frac{1}{d\phi} \left[x_t \sqrt{\sin \phi} \right]$$

$$= \frac{x_t}{\cos \phi} \frac{\cos \phi}{2 \sqrt{\sin \phi}} = \frac{x_t}{2 \sqrt{\sin \phi}} \tag{30}$$

$$\rho_c = \frac{x}{\sqrt{\sin \phi}} \tag{31}$$

Substituting Equations (28), (30) and (31) into Equation (29) and solving for f_c yields

$$f_c = p\,\rho_c - \frac{\rho_c}{\rho_m} f_m = \frac{px}{\sqrt{\sin \phi}} - \frac{2}{x_t}\left[\frac{px}{2 \sin \phi}\right]$$

$$= \frac{px}{\sqrt{\sin \phi}} - \frac{px}{x_t \sin \phi}$$

But,

$\frac{x}{x_t} = \sqrt{\sin \phi}$ (by Equation 20). Therefore,

$$f_c = \frac{px}{\sqrt{\sin \phi}} - \frac{px}{\sqrt{\sin \phi}} = 0 \tag{32}$$

The Taylor's curve as given by Equation (20) is difficult to plot. However, it may be expressed in cartesian coordinates by means of elliptic functions which have been tabulated. The mathematics involved in the conversion are not shown herein but are given in Reference 1. Tables of the resulting cartesian coordinates at various points along the curve are presented in References 1 and 7. The values from Reference 7 were used in determining the shape of the end closure as shown in Figure 1. The coordinates in terms of the major semi-axis and the tangency cut-off point are shown in Table I. The tangent to the curve is parallel to the transition conical frustum, e. g.

$$\frac{\pi}{2} - \phi_o = \theta \tag{33}$$

1. Meridional Cables

The structural elements ... the dome are N = 480 meridional cables. These are 1/16-inch, 7 x 7, flexible carbon steel cables having an ultimate tensile strength of F_{tu} = 480 lb (Reference 8).

Since the cable spacing is $2\pi x/N$, the load in each cable is (refer to Equation 28):

$$T_m = \frac{2\pi x}{N} f_m = \frac{p\pi x^2}{N \sin \phi} \tag{34}$$

By considering Equations (34) and (27) it is evident that the cable tension is constant everywhere.

Substituting the following values into Equation (34),

$x = x_o = 47.75$ in.

$\phi = \phi_o = \frac{\pi}{2} - \theta = 75^o$, $\sin \phi_o = 0.96593$

$N = 480$

$$\frac{T_m}{p} = \frac{(47.75)^2 \pi}{(480)\,(0.96593)} = 15.40 \text{ in.}^2 \tag{35}$$

Table I. Coordinates of the Zero Circumferential Stress, Isotensoid Meridian Dome

Unit Coordinates (From Reference 7)		
x	y	ϕ (Degrees)
0	0.59907	0.0
0.1	0.59875	0.573
0.2	0.59640	2.292
0.3	0.59005	5.164
0.4	0.57762	9.207
0.5	0.55683	14.478
0.6	0.52494	21.100
0.7	0.47806	29.341
0.8	0.40946	39.732
0.9	0.30296	54.096
1.0	0.0	90.0
Cut-Off Iteration		
0.96	0.19666	---
0.97	0.17104	---
0.98	0.14024	---
0.98282	0.12877	75.0
0.99	0.09958	78.55

For the design limit pressure of 5 psi and using a factor of safety of F.S. = 3 applied to the ultimate cable strength, the margin of safety is

$$M.S. = \frac{F_{tu}}{(F.S.)(T_m)} - 1 = \frac{480}{(3)(5)(15.40)} - 1 = +1.08$$

The above calculation assumes that the cable can develop 100 percent of its ultimate strength in this application. A reduced cable efficiency of 90 percent will be applied because:

(1) There is a small bend radius of 0.156 inch at the loops located on the large ring of radius x_o.

(2) There may be kinks induced in the cables during deployment.

The calculation is based on the results of preliminary tests of flexible carbon and flexible corrosion resisting steel cables which were subjected to "hard" kinks and yielded 90 and 75 percent efficiencies, respectively. The reduced margin of safety is then,

$$M.S. = (2.08)(0.9) - 1 = +0.87$$

2. Cable Connection Test Results

A 4-1/2 x 3 x 1-1/4 inch, 4130 steel piece (shown in Sketch C) was machined to the cross section of the ring and then heat treated to F_{tu} = 150 ksi. Because of the inferior test specimen (the pin was inserted on an angle as shown), there was a nonuniform load distribution due to the resulting variable cable lengths. Therefore, one loop (two cables) located on the short side failed prematurely at a total axial load of 10,900 lb. The remaining 14 loops then failed simultaneously at a total axial load of 12,600 lb. Since the breaking strength

Sketch (C)

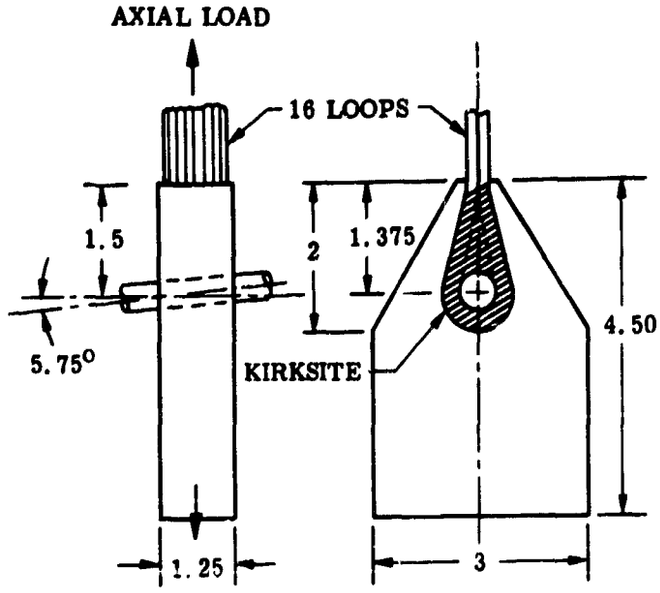

is given in Reference 8 as 480 lb per cable, this corresponded to an efficiency of 93.75 percent. In addition, no yielding of the Kirksite matrix or of the fitting was observed. The test results are considered to be an adequate verification of the strength of this fitting.

C. ACCORDION FABRIC CYLINDER

The cylinder is composed of N = 244 longitudinal fabric straps that are unsupported in the circumferential direction. They are alternately laced to a series of hoop cables of two different diameters, thus forming an unloaded accordion shape (see Figure 1).

Since, under the operating and proof pressures of 5 and 10 psi respectively, the straps take large deflections, the deflected shape must be determined in order to calculate the fabric stresses and the hoop cable loads.

Preliminary investigation showed certain geometric constraints. Since the flexible hoop cables can resist radial tensile loads only, and since the inner diameter and the length of the cylinder are prescribed, there exists a maximum allowable diameter of the outer hoop cables for which they will remain in tension. The design approach is to first omit all the outer hoop cables and to determine the nonextensible shape (the shape that the cylinder takes at very low inflation pressures since the stretch of the fabric is taken as zero). The outer hoop cables are then placed on this deformed shape at the desired locations as dictated by packaging considerations. The extensible shape of the cylinder is next calculated for both the operating and the proof inflation pressures.

1. Nonextensible Shape

Since this shape is independent of the magnitude of the inflation pressure and since the straps are laterally unsupported, only one strap under a general uniform load, w, need be considered.

Assume the load is uniformly distributed so that the deformed curve is an arc of a circle.

Sketch (D)

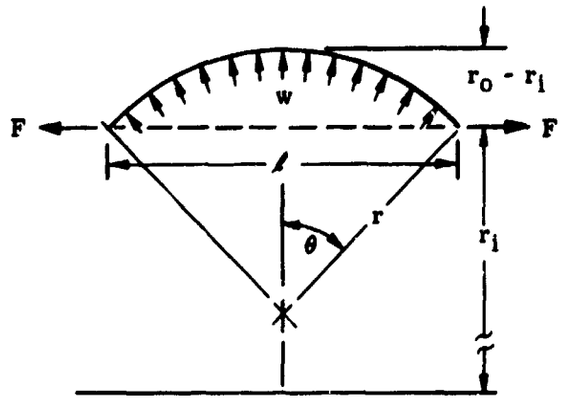

For static equilibrium,

$$r \cos \theta = \frac{F}{w} \tag{36}$$

From geometry, shown in Sketch (D),

$$r \sin \theta = \frac{\ell}{2} \tag{37}$$

From Equations (36) and (37),

$$\theta = \tan^{-1} \frac{w\ell}{2F} \tag{38}$$

But,

$$F = \frac{\pi}{N} p r_i^2 \tag{39}$$

And, as a first approximation,

$$w = \frac{2\pi}{N} p r_i \tag{40}$$

From Equations (39) and (40), $\frac{w}{F} = \frac{2}{r_i}$ (41)

Substituting Equations (41) into (38) yields,

$$\theta = \tan^{-1} \frac{\ell}{r_i} \tag{42}$$

It then follows, from equation (37), that

$$r = \frac{\ell}{2 \sin \theta}$$

and

$$r_o - r_i = r (1 - \cos \theta) = \frac{\ell(1 - \cos \theta)}{2 \sin \theta} \tag{43}$$

Using the desired inner hoop radius and spacing, r_i and ℓ, determine θ from Equation (42), and determine r_o from Equation (43). A second approximation of the distributed load is,

$$w = \frac{\pi}{N} p (r_i + r_o) \tag{44}$$

and,

$$\frac{w}{F} = \frac{r_i + r_o}{r_i^2} \tag{45}$$

Substituting Equations (45) into (38) yields

$$\theta = \tan^{-1} \frac{\ell (r_i + r_o)}{2 r_i^2} \tag{46}$$

Determine a second value of θ from Equation (46) and determine a new r_o from Equation (43). A third value of θ is then determined from Equation (46) and the process is repeated until the value of r_o is stabilized. The nonextensible arc length that the cylinder is fabricated to is then $2r\theta$ with the value of r determined from Equation (37).

The outer hoop cables are now placed upon this nonextensible shape as shown in Sketch (E):

Sketch (E)

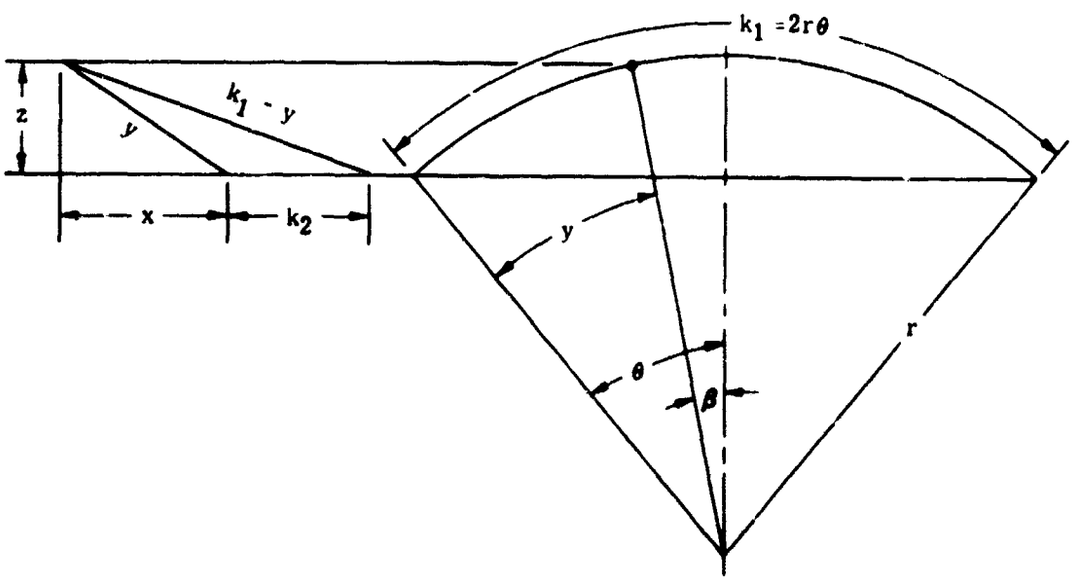

k_2 is established by packaging considerations.

From geometry,

$$\beta = \theta - \frac{y}{r} \tag{47}$$

$$z = r(1 - \cos\theta) - r(1 - \cos\beta) = r(\cos\beta - \cos\theta)$$

$$= r\left\{\cos\left|\theta - \frac{y}{r}\right| - \cos\theta\right\} = r\left\{\left|\cos\frac{y}{r} - 1\right| \cos\theta + \sin\frac{y}{r}\sin\theta\right\} \tag{48}$$

$$y^2 - x^2 = z^2 \tag{49}$$

$$(k_1 - y)^2 - (x + k_2)^2 = z^2 \tag{50}$$

Equate (49 and 50), $(k_1 - y)^2 - y^2 - (x + k_2)^2 + x^2 = 0$

$$k_1^2 - 2k_1 y - k_2^2 - 2k_2 x = 0$$

$$x = \frac{k_1^2 - k_2^2 - 2k_1 y}{2k_2} \tag{51}$$

From Equations (48) and (49),

$$x^2 = y^2 - z^2 = y^2 - r^2\left\{\left|\cos\frac{y}{r} - 1\right| \cos\theta + \sin\frac{y}{r}\sin\theta\right\}^2 \tag{52}$$

Assume values of y and plot x versus y for both Equations (51) and (52). The intersection of the curves gives the proper values of x and y. Using these values, z is found from Equation (49), and the outer hoop cable radius is

$$r_{oc} = r_i + z \tag{53}$$

The calculations are not shown, but the cylinder values are given as follows:

r = 49.7 in.
N = 244
r_i = 44.5 in.
r_o = 52.0 in.
r_{oc} = 51.0 in.
θ = 31.55°
β = 0.03°
x = 25 in.
y = 25.9 in.
K_2 = 3 in.
K_1 = 54.7 in.
z = 6.5 in.

2. Extensible Shape

a. Experimental Load-Deflection Data. Since lighter webbing was not readily available early in the program, two test specimens of 3600 lb/Dacron webbing were loaded in a universal testing machine with elongations measured manually between gage marks on the specimens. The measured elongations are recorded in Table II with their respective load levels and the calculated moduli of elasticity. The load-deflection data is also shown in Figure 11 including a sketch of the test specimen.

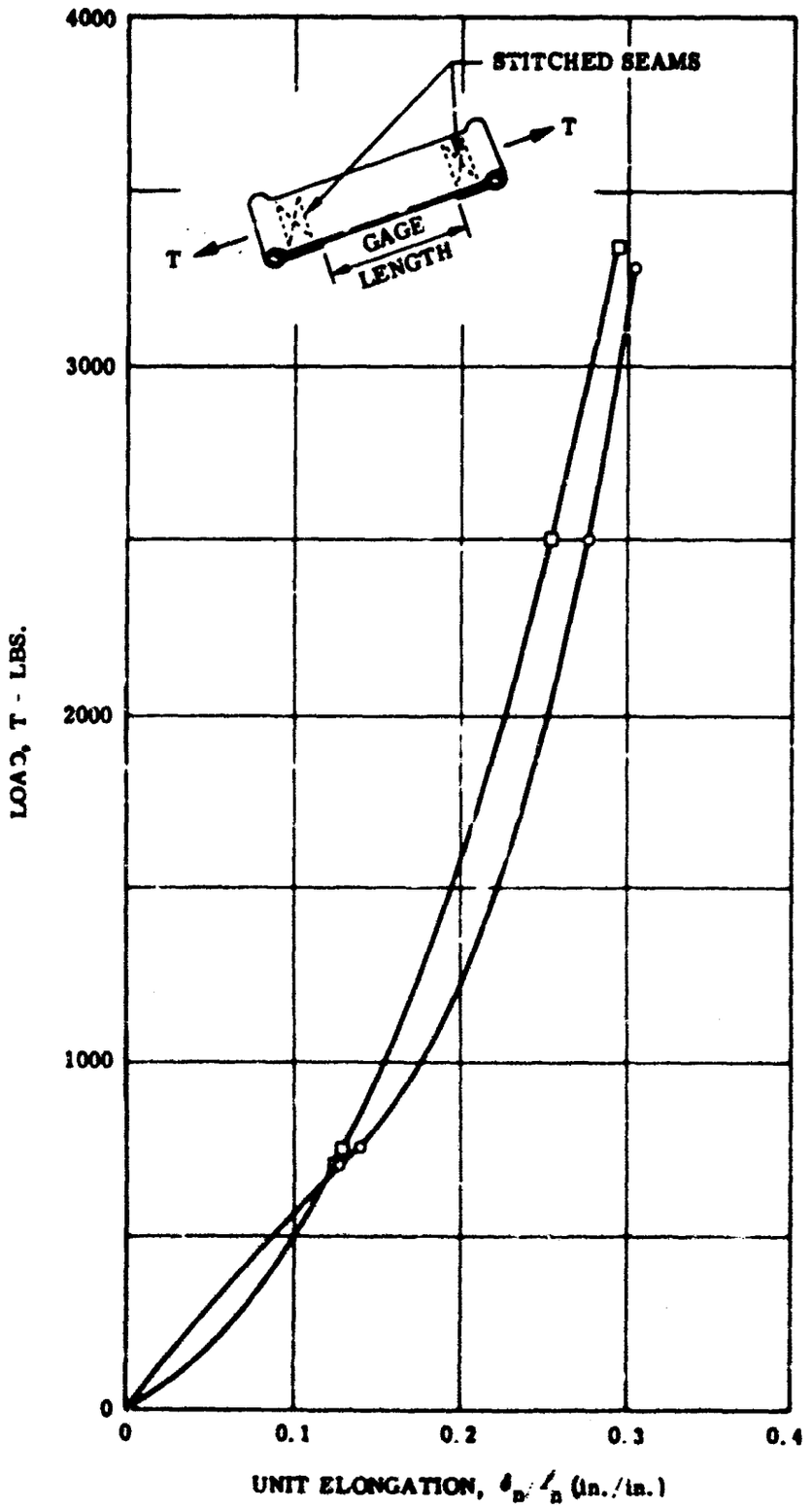

Figure 11. Load Deflection Data for the Dacron Straps

Table II. Results of Dacron Strap Tests

Spec No.	Load (Lbs)	Incr Load (Lbs)	Length (In.)	Elongation (In.)	Incr Elongation (In.)	Unit Elongation (In./In.)	Incr Unit Elongation (In./In.)	Tangent Modulus E_t (Lbs)	Secant Modulus E_s (Lbs)
1	0	---	14.25	0	----	----	----	----	----
	---	700	----	----	1.8125	----	0.1272	5503	----
	700	---	16.0625	1.8125	----	0.1272	----	----	5503
	---	50	----	----	0.1875	----	0.01316	3799	----
	750	---	16.25	2.00	----	0.1404	----	----	5342
	---	1750	----	----	1.9375	----	0.13596	12871	----
	2500	---	18.1875	3.9375	----	0.2763	----	----	9048
	---	780	----	----	0.4375	----	0.03070	25407	----
	3280	---	18.625	4.375	----	0.3070	----	----	10684
2	0	---	13.50	0	----	----	----	----	----
	---	700	----	----	1.6875	----	0.1250	5600	----
	700	---	15.1875	1.6875	----	0.1250	----	----	5600
	---	50	----	----	0.0625	----	0.00463	10799	----
	750	---	15.25	1.75	----	0.1296	----	----	5787
	---	1750	----	----	1.6875	----	0.125	14000	----
	2500	---	16.9375	3.4375	----	0.2546	----	----	9819
	---	840	----	----	0.5625	----	0.0417	20144	----
	3340	---	17.5	4.0	----	0.2963	----	----	11272

b. Section Analysis. The initial geometry is that of the nonextensible case.

(1) Left-Hand Lobes. First consider the extensible deformations of the short arc of initial length, y, between the inner and the outer hoops. In Sketch (F), the dashed lines and the solid lines represent the initial and the deformed geometry respectively.

Given:

$$w = \frac{\pi p}{N}(r_i + r_o) \qquad \text{(Reference Equation (44))}$$

$$\frac{w}{F} = \frac{r_i + r_o}{r_i^2} \qquad \text{(Reference Equation (45))}$$

$$r_\theta = r$$

The initial strap tensions for 5 and 10 psi are

$$T_5 = w_5 r_\theta$$

$$T_{10} = 2T_5 \qquad (54)$$

The corresponding strains are ϵ_5 and ϵ_{10} respectively. The stretched arc lengths are then

$$2(r_y \gamma)_5 = y(1 + \epsilon_5)$$

$$2(r_y \gamma)_{10} = y(1 + \epsilon_{10}) \qquad (55)$$

Sketch (F)

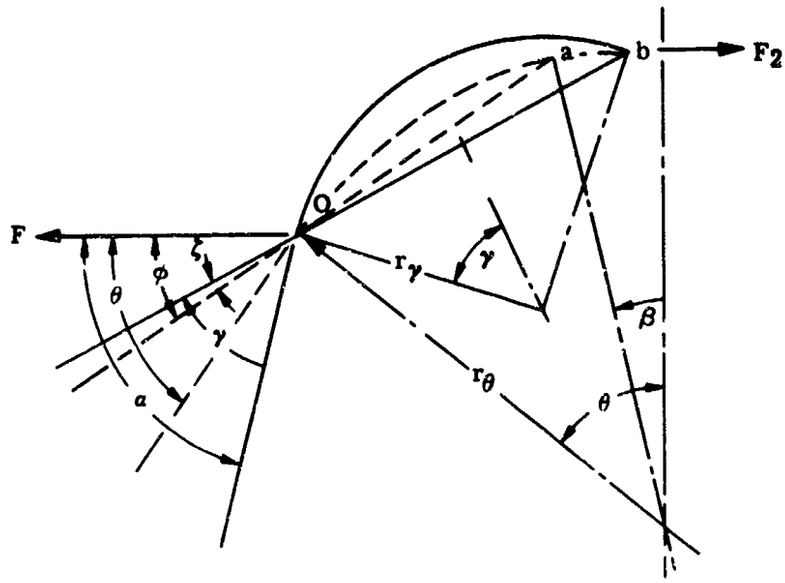

In the preceding sketch, the angle, ϕ, may be determined from the results of the nonextensible analysis as,

$$\phi = \sin^{-1}\left[\frac{z}{2r_\theta \sin\left[\frac{\theta - \beta}{2}\right]}\right] \tag{56}$$

For equilibrium,

$$r_\gamma \cos\alpha = \frac{F}{w} \tag{57}$$

From geometry,

$$\alpha = \phi - \zeta + \gamma \tag{58}$$

and

$$\frac{\sin(\phi - \zeta)}{r_\phi \sin\left[\frac{\theta - \beta}{2}\right]} = \frac{\sin\phi}{r_\gamma \sin\gamma} \qquad \text{(Reference } \Delta 0ab) \tag{59}$$

Eliminating r_γ from Equations (55) and (57),

$$\left.\begin{aligned}\left[\frac{\gamma}{\cos\alpha}\right]_5 &= \frac{y(1+\epsilon_5)(r_i + r_o)}{2r_i^2} = C\epsilon_5 \\ \left[\frac{\gamma}{\cos\alpha}\right]_{10} &= \frac{y(1+\epsilon_{10})(r_i + r_o)}{2r_i^2} = C\epsilon_{10}\end{aligned}\right\} \tag{60}$$

Substituting for $(\phi - \zeta)$ and for r_γ from Equations (58) and (55), respectively, into Equation (59) yields,

$$\left.\begin{aligned} \sin(\alpha - \gamma)_5 &= \frac{2r_\theta}{y(1+\epsilon_5)} \sin\left[\frac{\theta-\beta}{2}\right] \sin\phi \ \frac{\gamma}{\sin\gamma} = K_{\epsilon 5} \frac{\gamma}{\sin\gamma} \\ \sin(\alpha - \gamma)_{10} &= \frac{2r_\theta}{y(1+\epsilon_{10})} \sin\left[\frac{\theta-\beta}{2}\right] \sin\phi \ \frac{\gamma}{\sin\gamma} = K_{\epsilon 10} \ \frac{\gamma}{\sin\gamma} \end{aligned}\right\} \quad (61)$$

Eliminating γ from Equations (60) and (61) yields,

$$\sin(\alpha - C_\epsilon \cos\alpha) = K_\epsilon \sin\frac{\epsilon \cos\alpha}{(C_\epsilon \cos\alpha)} \quad (62)$$

Let

$$\lambda = C_\epsilon \cos\alpha \quad (63)$$

Equation (62) then becomes

$$\sin(\alpha - \lambda) = K_\epsilon \frac{\lambda}{\sin\lambda} \quad (64)$$

Using factors of safety of 5 on the working pressure (5 psi) and 2-1/2 on the proof pressure (10 psi), the corresponding strains from Figure 11 are $\epsilon_5 = 0.07$ and $\epsilon_{10} = 0.12$. Using these strains and values from the nonextensible shape, values are determined for C_ϵ and K_ϵ from Equations (60) and (61) respectively. Then α is determined from Equations (63) and (64) by trial and error using tables of the $\sin\lambda/\lambda$ functions. The calculations are not shown, but the values of α and the strap tensions are given as follows:

$\alpha_5 = 40.36^\circ$

$\alpha_{10} = 40.37^\circ$

$T_5 = w_5(r_\gamma)_5 = 132$ lb

$T_{10} = w_{10}(r_\gamma)_{10} = 264$ lb

The force that is transverse to the plane of the outer hoops and ties the left and right-hand lobes together is denoted F_2 and is determined as follows in sketch (G):

For 5 psi,

$$F_2 = 132 \cos 1.86^\circ = 132 \text{ lb.}$$

For 10 psi,

$$F_2 = 264 \cos 0.13^\circ = 264 \text{ lb.}$$

(2) Right-Hand Lobes. The remaining part of the repeating sections to be analyzed is the long arc of initial length, $(k_1 - y)$, using Sketch (H).

Proceeding in a similar manner to that used for the left-hand lobes, the strap tensions are determined. The tensions are given as follows:

$\alpha_5 = 6.50^\circ$

$\alpha_{10} = 8.43^\circ$

$T_5 = w_5(r_\gamma)_5 = 133$ lbs

$T_{10} = w_{10}(r_\gamma)_{10} = 267$ lbs

Sketch (G)

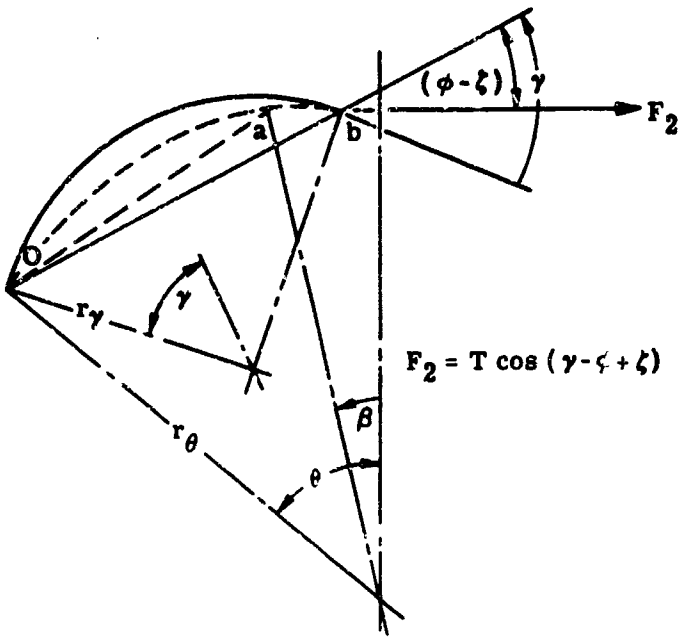

$$F_2 = T \cos(\gamma - \varsigma + \zeta) \qquad (65)$$

Sketch (H)

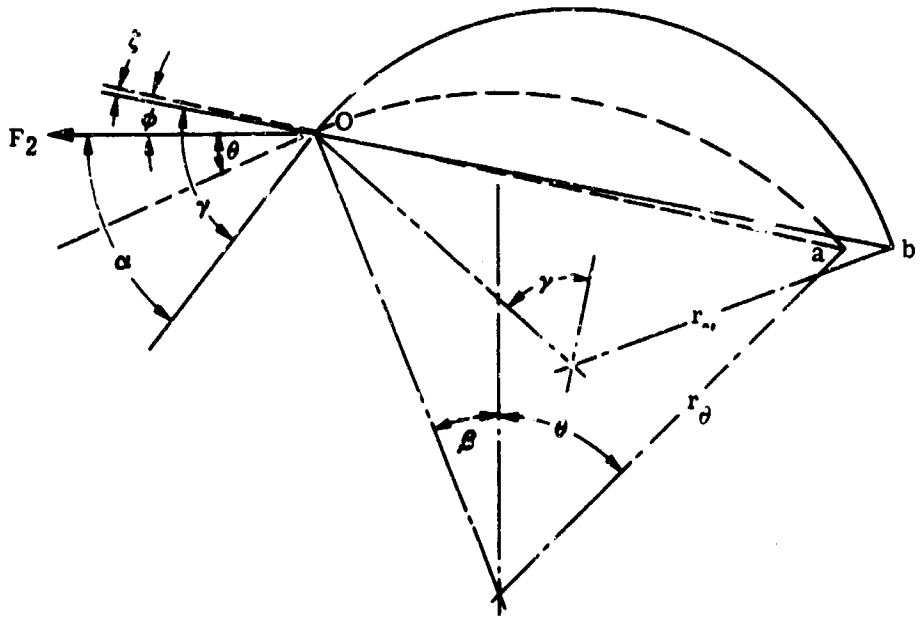

The maximum tension for an inflation pressure of 5 psi is thus 133 lb in the right hand lobes of the straps. For a factor of safety of 5, the required strap strength is 665 lb.

The force that is transverse to the plane of the outer hoops and ties the left and right-hand lobes together is F_2 and is given as follows:
For 5 psi,

$$F_2 = 133 \cos 6.50^{\circ} = 132 \text{ lb.}$$

For 10 psi,

$$F_2 = 267 \cos 8.43^{\circ} = 264 \text{ lb.}$$

These values are in agreement with those for the left-hand lobe.

3. Analysis of Hoop Cables

Each hoop cable is composed of n strands of 0.080-inch diameter steel wire. The minimum ultimate tensile strength is F_{tu} = 282 ksi as specified in MIL-W-470. The minimum ultimate tensile load per strand, as based on the specified diameter variation of ±0.001 in., is therefore,

$$T_{tu} = \frac{\pi d^2}{4} F_{tu} = \frac{\pi}{4}(0.079)^2 (282 \times 10^3) = 1382 \text{ lb.}$$

A factor of safety of 3 will be used on the operating pressure loading of 5 psi.

The cable tension is simply $T_c = PR$ where R is the radius of the cable and P the radial loading. Letting the subscripts ℓ and r denote the left and right-hand straps that are connected to a hoop, the radial hoop loading, for N straps, is given by

$$P = (T_\ell \sin \alpha_\ell + T_r \sin \alpha_r) \frac{N}{2\pi R} \sim \text{lb/in.} \tag{66}$$

and

$$T_c = (T_\ell \sin \alpha_\ell + T_r \sin \alpha_r) \frac{N}{2\pi} \sim \text{lb} \tag{67}$$

For

$$N = 244, \quad T_c = 38.8 (T_\ell \sin \alpha_\ell + T_r \sin \alpha_r) \tag{68}$$

Taking the values for T and α from the extensible shape discussion, the inner and outer cable loads and the corresponding margins of safety based on factors of safety of 3 for the 5 psi operating load and 1.5 for the 10 psi proof pressure are determined in Table III.

Investigation of the wire termination details shows that all the coils in the cables will not be effective. Since the cables are wrapped every 12 inches it is doubtful that even 100 percent of the effectiveness of the last coil will be lost. However, to be conservative, arbitrarily let 20 percent of the coils in each cable be 100 percent ineffective. Then, the minimum margins of Table III are reduced to,

$$\text{30 coil cable, M.S.} = \left[\frac{24}{30}\right](2.0) - 1 = +0.6$$

$$\text{5 coil cable, M.S.} = \left[\frac{4}{5}\right](2.9) - 1 = +1.3$$

Table III. Hoop Cable Loads and Margins of Safety

Cable	p (psi)	n	n T_{tu} (Lb)	α_ℓ (Deg)	α_r (Deg)	T_ℓ (Lb)	T_r (Lb)	T_c (Lb)	M.S.
Inner Cable	5	30	41,460	40.73	40.36	133	132	6,684	+1.0
	10			41.03	40.37	267	264	13,436	+1.0
Outer Cable	5	5	6,910	1.86	6.50	132	133	750	+2.0
	10			0.13	8.43	264	267	1,542	+1.9

4. Bladder

The specified ultimate tensile strength and breaking elongation as supplied by the G. T. Schjeldahl Co. for the X660 cloth-laminate bladder are,

Warp direction, F_{tu} = 64 lb/in., ϵ_u = 22 percent

Fill direction, F_{tu} = 72 lb/in., ϵ_u = 29 percent

Since the bladder must span between meridional cables in the end closure and the fabric straps in the quasi-cylindrical part of the shelter, the maximum allowable spacing, ℓ, between these elements will be determined. Consider a one inch wide strip of the initially flat bladder to deform into a circular arc under the ultimate inflation pressure as shown in Sketch (I).

Sketch (I)

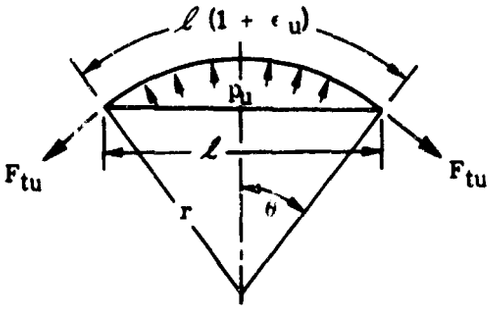

By equilibrium,

$$F_{tu} = p_u r \tag{69}$$

From geometry,

$$2 r \theta = \ell(1 + \epsilon_u) \tag{70}$$

$$2 r \sin\theta = \ell \tag{71}$$

Substituting the first two terms of the sin θ series and solving Equations (69), (70) and (71) for ℓ yields,

$$\ell = \frac{2 F_{tu}}{p_u (1 + \epsilon_u)} \sqrt{\frac{6 \epsilon_u}{1 + \epsilon_u}} \tag{72}$$

Substituting,

$$p_u = (F.S.)\,(p) = (5)\,(5) = 25 \text{ psi}$$

$$F_{tu} = 64 \text{ lb/in.}$$

$$\epsilon_u = 0.22 \text{ in./in.}$$

$$\ell = \frac{(2)\,(64)}{(25)\,(1.22)} \sqrt{\frac{(6)\,(0.22)}{1.22}} = 4.197\sqrt{1.0820} = (4.197)\,(1.0405) = 4.37 \text{ in.}$$

The maximum strap spacing occurs at the attachment to the support ring. The cc spacing between fittings is 4.263 in. Since there are two loops (4 straps) between fittings, one loop failure still allows a positive margin of safety on the bladder, i.e.,

$$\text{M.S.} = \frac{4.37}{4.263} - 1 = +0.02$$

Similarly, if 3 loops (6 meridional cables) fail in the end closure the bladder must span 4.008 inches and the resulting margin of safety is

$$\text{M.S.} = \frac{4.37}{4.008} - 1 = +0.09.$$

SECTION IX

MATERIALS SELECTION

A. INTRODUCTION

The composite material construction described was selected as most suitable for a space maintenance hangar. The candidate composite wall construction provides materials that have exceptionally good properties of low specific weight (0.600 lb /sq ft), impermeability to gases, resistance to solar and ultraviolet degradation, low surface vaporization due to the effect of a space vacuum. All are nontoxic. Based on this investigation, polymeric-type films, foam, fibers and elastomer materials, and certain ferrous and nonferrous-type materials, were selected for construction of the hangar composite structure. Materials selection, testing, and fabrication techniques described were developed under in-house company funded programs. The results of this in-house effort as it applies to this contract effort are presented.

B. COMPOSITE MATERIALS SELECTION

1. General

The lay-up construction of the composite structure utilized in the hangar fabrication is shown schematically in Figure 12 and the materials used in the manufacturing were as follows:

(1) Thermal Control Layer - Pigmented Silicone Paint

(2) Outer Cover Laminate - Nylon Cloth (Travis Mills Style 5096), Polyester Adhesive (G. T. Schjeldahl Company GT-201), Capran Film (Allied Chemical Type 77-C)

(3) Polyester Adhesive Binder Layer (Typical) - Vitel PE-207 (Goodyear Tire and Rubber Company)

(4) Micrometeoroid Barrier - 2-inch thick polyether foam (Nopco Chemical UU-15)

(5) Structural Layer - Longitudinal Straps of Dacron (Bally Ribbon 8674), Meridional Cables of 1/16 Diameter Carbon Steel Cables

(6) Structural Layer Binder Adhesive - Topolic-Type Polyurethane (Goodyear Tire and Rubber Company)

(7) Pressure Bladder Foam Layer - 0.070-inch thick PVC Foam (Great American Industries Rubatex R-313-V)

(8) Pressure Bladder Nylon Cloth - Nylon cloth (Burlington Style 1632)

2. Pressure Bladder

As shown in Figure 12, a triple-seal gas pressure-bladder concept is utilized for construction of the hangar structure. Qualification testing of the pressure-bladder component demonstrated the basic material to be more than adequate for the design leakage requirements. Both the nylon cloth and film-cloth laminated fabric provides excellent flexibility with a high strength-to-weight ratio cloth and a low modulus film gas barrier, while the closed cell Vinyl foam provides a cushioned layer for puncture protection. Excellent ply-adhesion strength is obtained with the polyester adhesive-layer, with foam tear occurring on separation of the layers. Physical properties for the pressure bladder composite and component materials are shown in Table IV.

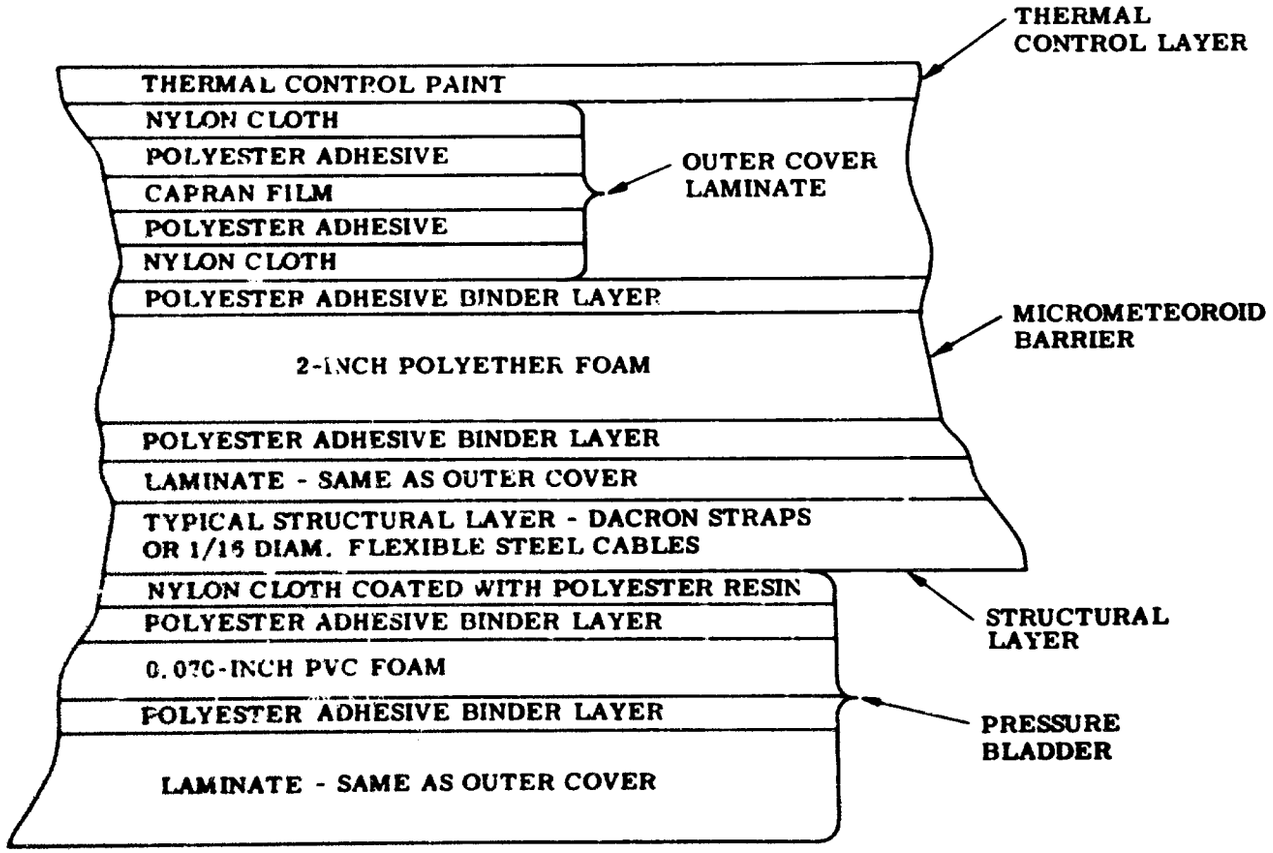

Figure 12. Schematic - Composite Wall Structure

Table IV. Physical Properties - Pressure Bladder

Material	Property
Nylon Cloth (Travis 5096)	
Weight, lb /ft^2	0.0063
Breaking Strength, lb /in - warp/fill	40/40
Thickness, Mils	2.5
Capran Film (Allied Chemical 77-C)	
Specific Gravity	1.13
Thickness, Mils	0.75
Ultimate Tensile, psi, MD	8500-11,500
TD	7000-11,000
Elongation, Percent, MD/TD	300-400
Tensile Modulus, psi, MD	90,000-110,000
TD	105,000-125,000
Nylon-Capran Laminate	
Weight, lb /ft^2	0.015 avg.
Breaking Strength, lb /in - warp/fill	72.0/60.0 min
Ply Adhesion, lb /inch	4.0 avg.
Thickness, Mils	6.75
Nylon Cloth (Burlington 1632)	
Weight, lb /ft^2	0.015
Breaking Strength, lb /in. - warp/fill	140/91
Thickness, Mils	4.7
PVC Foam	
Density, PCF	10.0-13.0
Temperature Resistance	
Low	-10°F
High Continuous	130° F
High Intermittent	200° F
Compression Set (ASTM Method)	
Compressed 50% - 22 hours at 70°F	50% maximum
Pressure Bladder Composite	
Weight, lb /ft^2	0.126 avg
Thickness, inches	0.0925
Ply Adhesion	Foam Tear
Permeability, (O_2), 5 psia, lb ft^2-24 hours	1.0 x 10^{-4}

3. Structural Layer

A lay-up construction utilizing Dacron fabric longitudinal straps and high-strength steel wire hoop cables was selected for the cylindrical section, and flexible carbon steel meridian cables for the end closure. Proper positioning of the flexible structural elements will be maintained by impregnating the polyurethane resin. Qualification testing of terminal end fittings for both the Dacron straps and meridian cables were conducted to demonstrate design efficiency. Physical properties of the flexible structural elements are shown in Table V.

Table V. Physical Properties - Flexible Structural Elements

Material	Property
Longitudinal Fabric Straps (Bally Ribbon 8674)	
Type	Dacron
Weight, oz/linear yard	0.23
Gage, inches	0.0114
Breaking strength, lb	675
Break Elongation, %	27.0
Hoop Cables	
Type	Steel Music Wire
Condition	Hard Drawn
Ultimate Tensile, psi, minimum	282,000
Size	0.080
Specification	MIL-W-470
Weight, lb /100 ft	1.69
Meridian Cables	
Type	Carbon Steel
Condition	Hand Drawn
Size	1/16 x 7 x 7
Specification	MIL-W-1511
Weight, lb /100 ft	0.75

4. Micrometeoroid Barrier

To provide the penetration resistance as determined by the micrometeoroid hazard assessment, 2-inch thick flexible polyether foam of 1.2 pcf density was selected (Figure 12). The polyether foam provides good elastic recovery characteristics for the exposure conditions required both before and after deployment. Also, exceptional ply adhesion is obtained in bonding to the other substrates.

5. Cover and Thermal Control Coating

An inner and outer cover fabric (Figure 12) of the same film-cloth laminated material, as described in the Pressure Bladder, is provided to encapsulate the entire 2-inch thick foam layer. This will permit pressurizing the 2-inch foam layer for enclosure expansion, and will permit exhausting of air from the foam layer prior to packaging, where required. A total of 4-mil dry thickness coating of silicone binder is painted on the outer cover surface with the proper pigmenting as determined in the thermal supporting analysis (Section VII) for thermal control.

C. FABRICATION TECHNIQUES AND PROCESSES

In fabricating the enclosure flexible wall structure, each component layer, as shown in Figure 12, is built up layer-by-layer starting with the pressure bladder on a partial male mandrel. The polyester adhesive binder layers bond the multiple-layer pressure-bladder components together, bond the outer cover to the two-inch foam layer, bond the structural layer multiple plies together, and bond the structural layer to both the two-inch foam layer and the pressure bladder. Thus the multiple plies are bonded into an integral and homogeneous structure. Physical properties for the bonding components are shown in Table VI.

Table VI. Physical Properties - Bonding Components

Item	Polyester	Polyurethane
Code	GT and R PE-207	GT and R Topolic
Type	Thermoplastic	Thermoset
Tensile, psi	7800	3000
Percent Elongation	100	480
Specific Gravity	1.2	1.1

D. MATERIALS TEST RESULTS AND EVALUATION

1. General

The materials selected for fabrication of the hangar composite structure were based on Goodyear Aerospace in-house sponsored development programs.

2. Weight

Actual weighing was conducted on the components of the composite structure with the following average weight breakdown results:

Construction		lb/ft^2
Thermal Control Paint		0.045
Outer Cover Laminate		0.015
Polyester Adhesive		0.027
2-inch Polyether Foam		0.200
Polyester Adhesive		0.027
Laminated Fabric		0.015
Longitudinal Straps (Incl. Adhesive Binder)		0.145
Pressure Bladder		
Nylon Cloth	0.015	
Polyester Adhesive	0.027	
0.070-inch PVC Foam	0.042	
Polyester Adhesive	0.027	
Laminated Fabric	0.015	0.126
Total		0.600

3. Pressure Tightness

To substantiate gas pressure tightness of the pressure bladder component material, permeability of samples were measured on Dow gas transmission cells in accordance with ASTM procedures. The tests were conducted at hangar deployment conditions of room temperature, 5 psia pressure, and gas atmosphere of 100 percent O_2. Permeability tests of "original" samples vs samples simulating the bladder splice joints showed only negligible leak rate change. Other permeability tests were made under the following sample conditions with the leak rate at pounds/foot^2 - 24 hours.

(1) Original Sample 1.0×10^{-4}

(2) Creased Sample 1.1×10^{-4}

(3) Punctured Sample - One Side 1.8×10^{-4}

4. Structural Integrity

To demonstrate structural integrity of the flexible structural layer, test samples of the termination joints were made and tested for both the longitudinal straps and meridian cables. Two Dacron strap joint samples were made as follows:

(1) 4-1/2 inch sewn seam length

(2) 6 point cross stitch

(3) 8-10 stitches per inch

(4) "F" type thread

(5) Sample gage length = 11.0 inches

Results of the two tests were as follows.

Sample No.	Ultimate Lbs/Inch	Type Failure
1	3980.0	At Seam
2	4030.0	At Seam

These heavy straps were tested since the desired weight was not available in time for the tests.

One sample test simulating the meridian cables apex joint was made. A sample encompassing 16 complete loops of 1/16 x 7 x 7 flexible steel cable terminating with Nicopress fittings and set in a steel fitting with Kirksite was made. All strands failed under an ultimate tensile load of 12,500 pounds

5. Temperature Control

To substantiate final requirements determined by the thermal analysis for space-stable thermal radiation properties of the thermal control layer, measurement of solar absorptance (α_s) and infrared emittance (ϵ) will be made before and after UV exposure under vacuum conditions with Goodyear Aerospace test facilities. Tests will consist of exposing the thermal control coating specimen to simulated solar radiation under vacuum at 10^{-7} torr or lower. The α/ϵ ratio and ϵ will be calculated from specimen data using radiometric and reflectometer measuring techniques.

6. Elastic Recovery

Time-load tests conducted on small samples of the micrometeoroid barrier foam layer were used to ascertain the maximum length of time the hangar can be packaged with a high reliability of elastic recovery when unpackaged. Figure 13 shows the recovery characteristics of the foam under vacuum conditions and for varying temperatures. From Figure 13 it can be seen that the packaged structure must be insulated against extreme cold if full recovery is to be achieved.

7. Environmental Effects

Tests on the composite wall material and its component layers under vacuum conditions

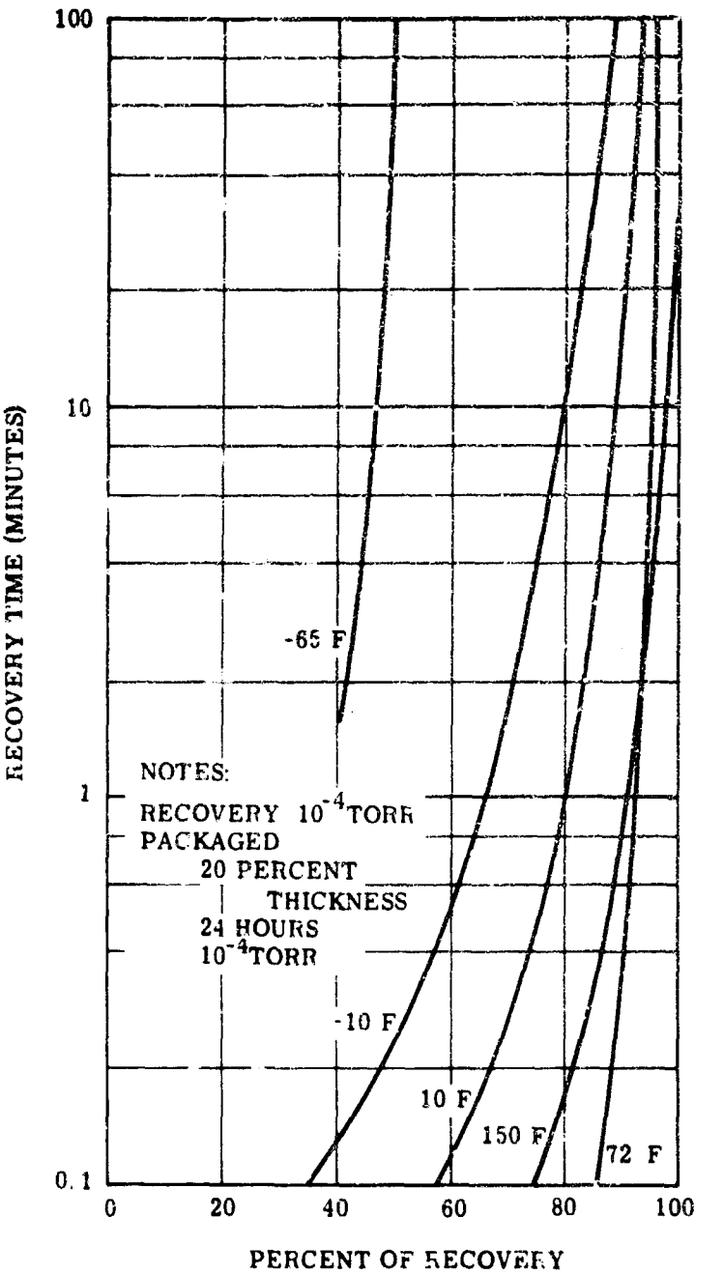

Figure 13. Foam Thickness Recovery Versus Time

Table VII. Vacuum Off-Gassing - Composite Wall Materials

Material	Percent Weight Loss	Time to Stabilize	Vacuum Level
Total Composite	2.63	40-Hrs	10^{-8} mm
Outer Cover	0.36	1.5	4×10^{-6}
2-Inch Foam	0.39	1.5	4.8×10^{-6}
Structural Layer (Longitudinal Straps)	0.12	1.0	10^{-6}
Pressure Bladder	6.3	36.0	10^{-6}

were used to evaluate off-gassing effects on the material physical properties (Table VII). An initial off-gassing is encountered resulting from boil-off of plasticizers and volatile solvents, with a negligible weight loss, which subsequently levels off.

8. Toxicity

Tests were made to assure that no toxic by-products, such as those used in the pressure bladder polymer type materials, are given off while under the deployment environment of 5 psia 0_2 atmosphere. A survey of toxic materials known to be used in the pressure bladder material construction was made, and found to be Toluene, Xylene, methylethyl ketone and Methylene Chloride solvents, also Toluene-diisocyanate (TDI). Although carbon monoxide was not known to be contained, tests for it were also included. The test procedure for collecting traces of any toxic gases was to place the test material in a pressure vessel that was evacuated and subsequently pressurized to 5 psia with 0_2. The test material was exposed for 24 hours, prior to chemical analysis of the toxic gases, and all were found to be below the threshold limit values for atmospheric contaminants established for occupational exposure. The values as determined by calorimeter-type chemical tester or mass spectrometer are shown in Table VIII.

Table VIII. Threshold Limits for Atmospheric Contaminants

Gases	Test Result Value (PPM)(1)	Threshold Limit Value (PPM)(2)
Toluene	200.0	200.0
Xylene	200.0	200.0
Methylethyl ketone	200.0	200.0
Methulene Chloride	200.0	500.0
Toluene-diisocyanate	0.01	0.02
Carbon Monoxide	25.0	100.0

(1) Values shown are minimum sensitivity values of instruments used in testing. In all cases, no trace of contaminants were found; therefore proving that if there were minute traces of contaminants, concentration is below threshold limit value.

(2) American Conference of Governmental Industrial Hygienists, 1963, or National Bureau of Standards

SECTION X

CONCLUSIONS AND RECOMMENDATIONS

A. CONCLUSIONS

The design aspects of a space maintenance hangar were investigated and practical solutions evolved under this contract.

The particular arrangment generated for the space maintenace hangar appears attainable within "current state of the art" and offers a potential for multiple mission applications. The design was also oriented towards integration compatibility with the Titan III C-MOL vehicle configuration. Vehicle integration was effected by incorporating a cylindrical adapter section, containing the packaged structure, between the MOL and the booster.

In addition to the design effort which was conducted, the supporting analysis portion of the program gave emphasis to the following:

(1) Structural analysis of the design indicates that the enclosure can be varied in length without causing major changes in the structure.

(2) Micrometeoroid studies, still being pursued on a company-funded basis, may enhance the protection capabilities of the structure in addition to reducing the weight by an appreciable amount.

(3) Thermal analysis indicated that the hangar hard structure can be used as a space radiator to help control internal temperatures.

(4) Packaging studies substantiated packageability of the hangar design within the configuration geometry of the launch vehicle, with the packaged structure including the canister occupying a space of only 4 feet in the longitudinal direction.

The study of specific mission applications for the space maintenance hangar, with their attendant design and operational constraints, was beyond the scope of this program effort. Studies for specific mission applications would entail the investigation of areas such as lighting, a more sophisticated thermal control system for maintaining a "shirt-sleeve" environment, associated operational equipment and fixtures from the confinement, weight, and structural loads aspects, and human factors limitations imposed by specific missions. Specific mission applications for the space maintenance hangar could include the following:

(1) Contained volume for conducting extra-vehicular activities experiments.

(2) Assembly facility for other satellite vehicles including assembly and checkout.

(3) Satellite intercept, acquisition, and disassembly.

(4) Sterilization of extra-terrestrial objects prior to earth return.

(5) Orbital supply and transfer station for mission extension.

B. RECOMMENDATIONS

Further detailed definition of the design is recommended. This definition would be directed towards the development of a maintenance hangar within accepted aerospace technology. Specifically, the following efforts are recommended as a logical extension of the subject program.

(1) Initiate studies of specific mission applications with respect to supplemental hardware installations, thermal control systems, structural loading possibilities, and human factors implications.

(2) Construct a scale model large enough to confirm design approach of the deployment and clam shell door operation systems.

(3) Fabricate a full-size hangar to static test the structural integrity and to demonstrate the operational aspects of the system.

SECTION XI

PROGRAM DEVELOPMENT PLAN

A. PREPROTOTYPE PROGRAM

The preprototype Space Maintenance Hangar Development Plan and Schedule is shown in Figure 14. The preprototype is scheduled for completion in 18 months. An additional four months is added to allow sufficient time to fabricate a canister and refurbish the hangar after testing in order to use the preprototype unit for compatibility checks. This unit would be available the 23rd month.

Emphasis will be placed on completing the preprototype design by the 6th month so that the unit can be fabricated and a series of tests started to verify design concepts. The test program will check out the ability of the hangar to take 5 psi pressure for long periods of time with only minor loss of pressurization gas. Packaging and deployment both in ambient and vacuum environments will also be important aspects of the preprototype test program.

B. PROTOTYPE PROGRAM

1. General

The prototype Space Maintenance Hangar Flight Hardware Plan and Schedule is shown in Figure 15. The prototype effort is scheduled to start the 16th month and is scheduled for completion the 33rd month. The program plan reflects a minimum type effort necessary for a flight article. Two units will be required for Qualification Testing. Unit 2 will be refurbished after completion of the Qualification Test and used as a standby unit. If this decision is not satisfactory, a 4th unit could be completed in the same length of time, since tooling will be available from Unit 2 to fabricate the 4th unit. Plans are to schedule 3 months for the refurbishment of Unit 2. This time could be spent on the fabrication of Unit 4.

2. Design

The prototype design overlaps the testing of the preprototype by 3 months. Effort can be started on the detailed design of the canister once the packaging tests are completed. Detail design of the hangar portion will be completed as the design concepts are verified during preprototype testing. The adapter design will be limited to defining constraints imposed on the adapter by the hangar design.

3. Quality Control and Reliability

A full-fledged Reliability & Quality Control Program will be conducted during the prototype design, fabrication and testing. Procurement and System Specifications will be written during the prototype program.

4. Fabrication

Three units are to be fabricated. Units 1 and 2 will be used for Qualification Testing and Unit 2 will be refurbished for delivery as a standby unit. Unit 3 will be the flight article.

The preprototype tooling will be refurbished and used for Units 1 and 3. One additional set of tooling will be fabricated for Unit 2. The fabrication area must be clean – free from dirt, metal shavings, splinters, etc. Environment must be controlled. A specific area will be set aside and improved for the fabrication of the hangar. Two sets of checkout equipment and 3 sets of handling equipment will also be fabricated for the prototype.

5. Testing

The test program will be designed to space qualify the hardware prior to flight test. The tests will include standard component and subsystem qualification, launch simulation and environmental tests, and additional testing in deployment and pressurizing of the hangar to ensure the quality and reliability of the completed product.

6. Delivery

The 3rd unit will be acceptance tested and ready for delivery 33-1/2 months after program go-ahead. The standby unit will be available for shipping the middle of the 35th month.

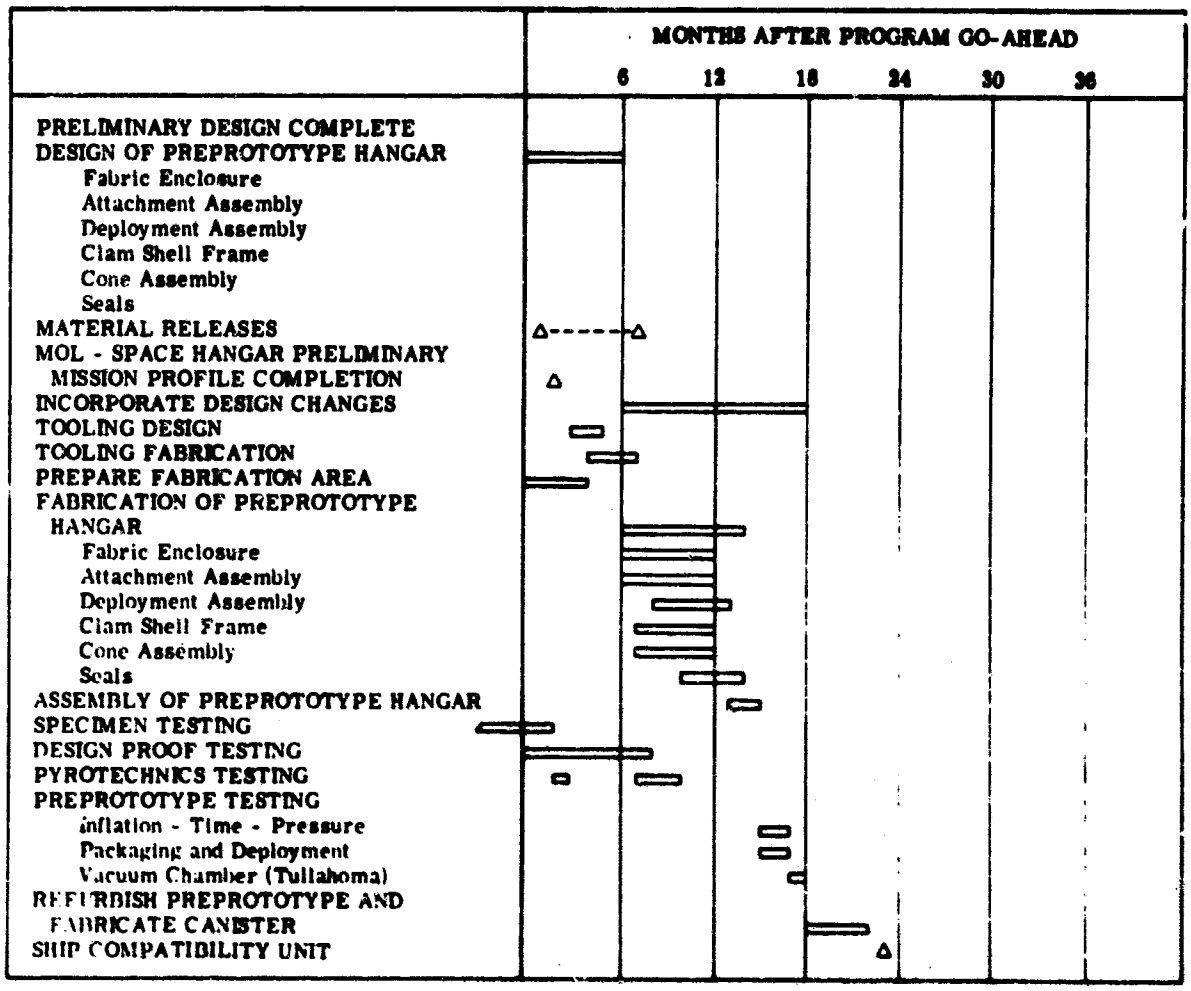

Figure 14. Space Maintenance Hangar Preprototype Development Plan and Schedule

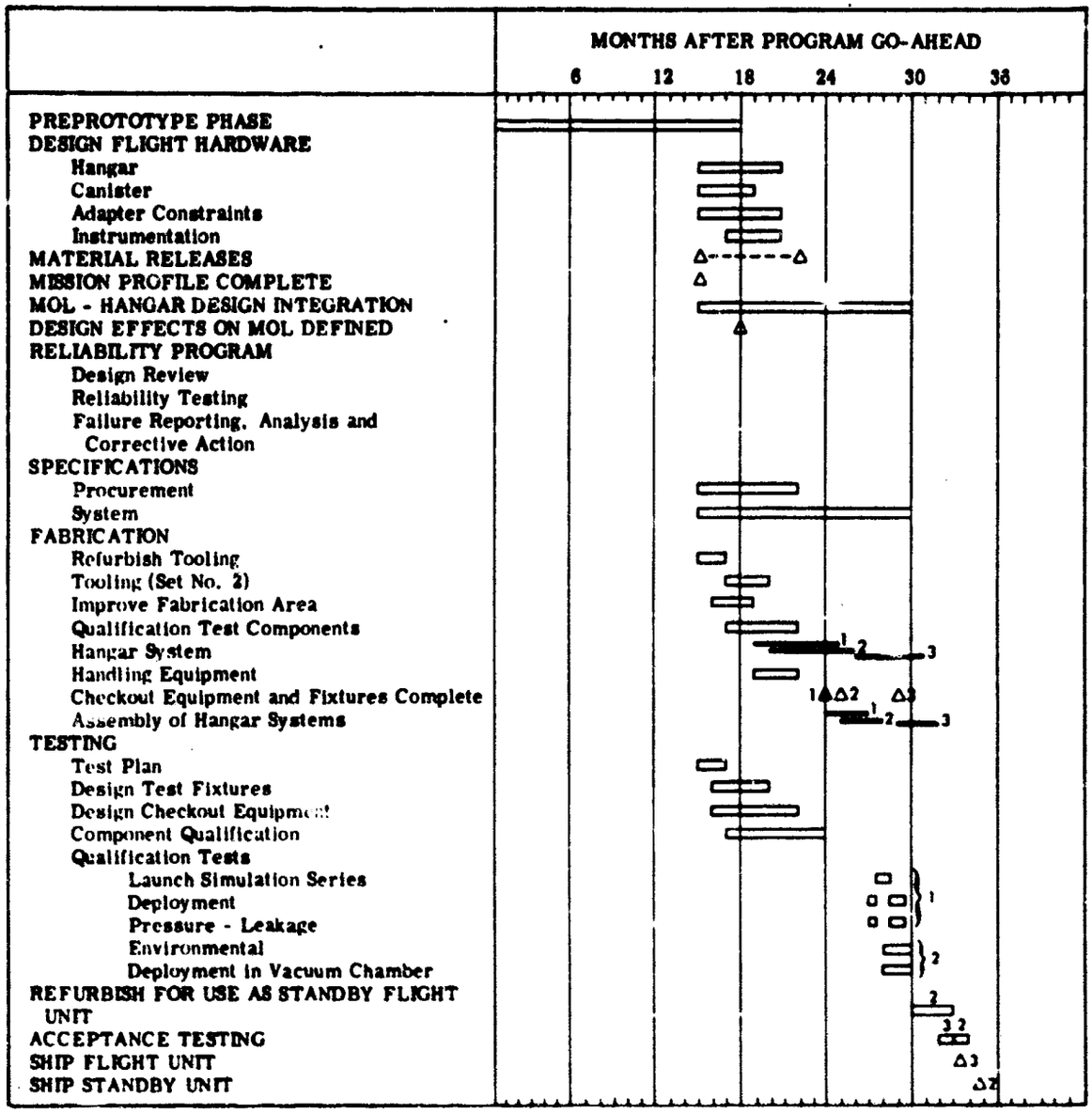

Figure 15. Space Maintenance Hangar Flight Hardware Plan and Schedule

REFERENCES

1. Jones, R; On the Aerodynamic Characteristics of Parachutes, Reports and Memoranda No. 862 (Ae 101) Aeronautical Research Committee, His Majesty's Stationary Office, London, June 1923

2. Meteoroid Environment in Near-Earth, Cislunar, and Near-Lunar Space, NASA Manned Spacecraft Center, Engineering Criteria Bulletin, EC-1, November 8, 1963

3. Hoffman, T. L.; Final Report, Expandable Gemini to MOL Crew Transfer Tunnel, GER-12335, Goodyear Aerospace Corporation, Akron, Ohio, December 1965

4. Reynolds, B. W., Effects of Hypervelocity Particle Impact on Composite Materials for Expandable structures Applications, Goodyear Engineering Report GER-10663, Akron, Ohio, August 1962

5. French, R. J., and et al., Development of Materials and Materials Application Concept for Joint Use as Cryogenic Insulation and Micrometeorite Bumpers Prepared for NASA under Contract NAS 8-11747 by Goodyear Aerospace Corp. GER-11676, June 1965

6. Timoshenko, S. and Woinowsky-Krieger, S.; Theory of Plates and Shells. Second Edition, McGraw-Hill Book Company, Inc., N. Y. 1959

7. Nourse, J. H. and Dennis, R. C.; The Ideal Geodesic Ovaloid Zero Axial Thrust, IBM 704 Computer Solutions, No. 2 Report, Hercules Powder Company, Allegheny Ballistics Laboratory, Cumberland, Maryland, August 1961

8. MIL-HDBK-5, "Metallic Materials and Elements for Flight Vehicle Structures", Department of Defense, Washington 25, D. C., August 1962